C_3H_6/NO_x Interactions Over a Diesel Oxidation Catalyst: Hydrocarbon Oxidation Reaction Pathways

by

Hyunsuk Oh

A thesis
presented to the University of Waterloo
in fulfillment of the
thesis requirement for the degree of
Master of Applied Science
in
Chemical Engineering

Waterloo, Ontario, Canada, 2012

AUTHOR'S DECLARATION

I hereby declare that I am the sole author of this thesis. This is a true copy of the thesis, including any required final revisions, as accepted by my examiners.

I understand that my thesis may be made electronically available to the public.

Abstract

C_3H_6 oxidation over a Pt/Al_2O_3 catalyst with or without NO_x present was investigated. In particular, its reaction mechanism was studied using diffuse reflectance infrared spectroscopy (DRIFTS), a reactor system designed for monolith-supported catalysts and a micro-reactor system designed for powder catalysts referred to as CATLAB. These experiments reveal that C_3H_6 oxidation is inhibited by the presence of NO, NO oxidation is inhibited by the presence of C_eH_6, and that adsorbed NO_x can react with gas phase C_3H_6. DRIFTS and CATLAB results confirm the reaction between C_3H_6 and nitrates, which are formed during NO_x adsorption, with linear nitrites observed as reaction products. Therefore, a reaction route is proposed for C_3H_6 oxidation in the presence of NO_x, namely, nitrates acting as oxidants. Using NO_2 instead of NO, or using a high NO_x/C_3H_6 ratio, which is beneficial for nitrate formation, favors this reaction pathway. Data also showed that Pt is required for this reaction, which suggests the nitrates in proximity to the Pt particles are affected/relevant.

Reaction kinetics studies of C_3H_6 oxidation over Pt/Al_2O_3 and Pt/SiO_2 catalysts were performed in CATLAB using a temperature-programmed oxidation method with different oxidants: O_2, NO_2 and nitrates. The reaction kinetics of these possible reactions were compared in order to determine which reaction is more important. NO_x adsorption does not occur on the SiO_2 surface so the reaction between C_3H_6 and NO_2 could be isolated and the effect of nitrates could be observed as well when compared to the results from Pt/Al_2O_3. The Pt dispersions were determined using H_2 chemisorption and were 1.3 and 1.6% for Pt/Al_2O_3

and Pt/SiO_2, respectively. C_3H_6 oxidation starts at a lower temperature with O_2 than with NO_2 but the activation energy was lower with NO_2. This gives indication that hydrocarbons must be activated first for NO_2 to be favored in hydrocarbon oxidation. When the experiment was done with C_3H_6 and nitrates, the reaction did not occur until NO_x started to desorb from the catalyst at higher temperatures, when nitrates become unstable and decompose. Therefore, O_2 was added to the system and the reaction began at even lower temperature than with just C_3H_6 and O_2. This proved that hydrocarbons need to be activated in order for surface nitrates to affect C_3H_6 oxidation and this reaction also resulted in a lower activation energy than with just C_3H_6 and O_2. Nitrate consumption was also observed as less NO_x desorbed from the catalyst at the later stage of the temperature ramp compared to the amount desorbed when the catalyst was not exposed to C_3H_6.

Acknowledgements

I would like to first thank my family and friends for their continuous support and encouragement. I would not have made it this far without them.

I would like to express my sincere gratitude to my supervisor Dr. William Epling for his patience, motivation and immense knowledge to help me push through and successfully complete my graduate studies. I want to also thank my colleagues John, Crystle, Iza, Ali and Suad for all their help and insightful discussions.

My sincere thanks also goes to Dr. Mark Pritzker and Dr. Zhongwei Chen for their time spent reviewing my thesis.

Furthermore, I would like to thank the Natural Sciences and Engineering Research Council of Canada (NSERC) and Cummins Inc. for their financial support.

Table of Contents

List of Figures

List of Tables

Chapter 1
Introduction

Air pollution has become a serious problem since the late 1960s and much effort has been made by government and industry to better control vehicle emissions. However, this has been offset by the increasing number of cars in the world. The dissatisfaction with the current state of the environment has caused environmental regulations regarding vehicle emissions to be made more rigorous [1]. A main problem is the fossil fuel combustion process in stationary and mobile sources, such as power plants and vehicles, respectively. Internal combustion engines, which are used for vehicles that consume gasoline or diesel fuel depending on the engine. Diesel fuel, which is a mixture of hydrogen and carbon molecules, is derived from crude oil. Unfortunately, it is impossible to have a clean combustion process when fossil fuels are involved. The key pollutants generated in this combustion process are sulfur oxides (SO_x), particulate matter (PM), which is often referred to as soot, carbon monoxide (CO), unburned hydrocarbons (HC) and nitrogen oxides (NO_x) [2]. The CO, unburned HC and PM emissions are produced from incomplete combustion while the NO_x is mostly formed from the reaction of nitrogen (N_2) and oxygen (O_2) in the air during combustion [3]. Other sources of HC in diesel exhaust are partially decomposed fuel molecules or recombined intermediate compounds, as well as lubricating oils [4]. Generally, only a low amount of CO remains from diesel combustion because it operates with an excess amount of air, so that oxidation proceeds primarily to CO_2. NO_x emissions regulations define two gases, nitric oxide (NO) and nitrogen dioxide (NO_2). In diesel engine exhaust, NO usually makes up about 70 – 90% of the total NO_x in the engine exhaust. NO_2 is very reactive and a strong oxidant [2], which is

an important property as it plays a role in the oxidation of HC, CO and soot in catalytic processes in the emission control system.

It has been reported by Environment Canada that passenger vehicles contribute about 21% of NO_x, 51% of volatile organic compounds (VOC) and 4% of particulate matter smaller than 2.5 micrometers (PM2.5) emissions in Canada [5]. These pollutants negatively affect the environment by leading to photochemical smog formation, acid rain and greenhouse gas effects and are also health threats to humans as well. As shown in Figure 1, light-duty vehicles, which represent passenger cars and light-duty trucks (weighing less than 8500 pounds), contributed about 63% of the greenhouse gas emissions from US transportation sources in 2006.

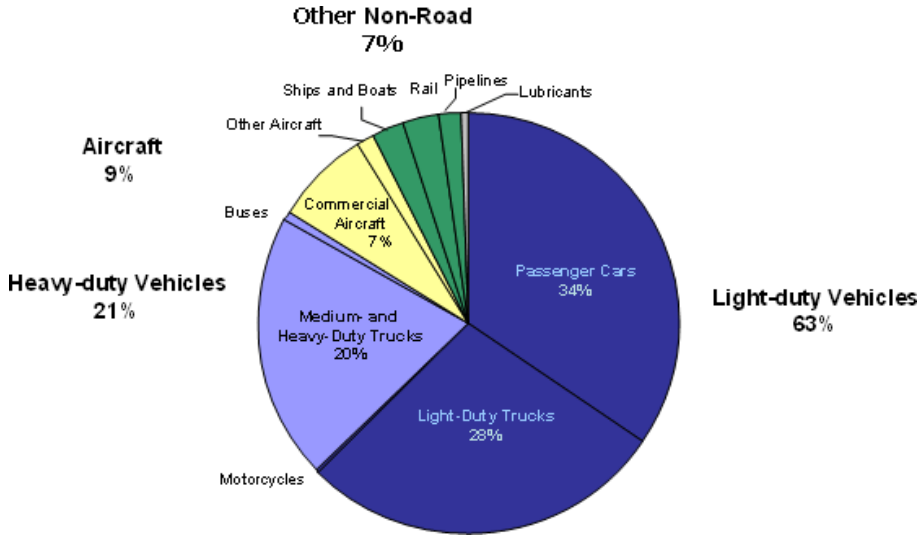

Figure 1: US transportation greenhouse gas emissions by source in 2006 [6].

Even though significant improvements have been made over the years to the engine, fuel and the exhaust control system [7], vehicles still continue to be a key source of harmful air pollutants.

Due to the negative effects these pollutants have on the environment and the increasing number of cars in the world, emission standards are put in place to help minimize the negative effect. The current emission regulations for internal combustion engines in Canada are governed by Environment Canada and Transport Canada [8]. The general approach for vehicle emission standards in Canada is to harmonize them with the US Environmental Protection Agency (EPA) federal standards as much as possible. The current emissions regulations came into effect under the Canadian Environmental Protection Act (CEPA) in September 1999, which continued its approach of alignment with the US EPA standards. While EPA regulates the federal emission standards in the US, the state of California has its own set of emissions regulations that are generally regarded as the stricter of the two [8]. Other states can make a choice to either follow the federal emissions standards or the California standards.

To keep up with these increasingly stringent restrictions, new technology and improvements to current automotive technology are necessary. One of the major technologies for vehicle pollutant emission removal is the catalytic converter. The purpose of the catalytic converter is to eliminate toxic and smog forming emissions of HC, CO and NO_x from the exhaust [9]. The current catalytic converter technology in gasoline-powered vehicles is the three-way catalyst (TWC), while diesel-powered vehicles use a combination of diesel oxidation

catalysts (DOCs), NO_x abatement systems and particulate filters. Gasoline-powered vehicles are widely available in North America while diesel-powered vehicles are not, although diesel-powered engines are more fuel efficient, reliable, durable and produce significantly less CO and HC emissions. However, since diesel engines produce more torque, they are primarily used for freight movers. Based on these advantages, diesel will continue to have a place in the transportation sector and could continue to become more popular as a source of fuel. For example, since European countries impose a higher fuel tax so it makes sense for diesel powered vehicles to be more widely available due to their better fuel efficiency [10].

Diesel and gasoline combustion engines use different catalytic control systems primarily due to their different operating conditions. Spark-ignited (SI) gasoline engines operate at a stoichiometric air to fuel ratio and TWCs are designed to perform well in this setting, which is relatively O_2 free. On the other hand, since diesel engines operate under lean conditions, which means an excess of air relative to the stoichiometric amount required for fuel combustion, TWCs cannot function efficiently in this condition. Specifically, the excess air creates an O_2-rich exhaust environment, making NO_x reduction challenging. A DOC is used to oxidize the HC and CO species to CO_2 and H_2O as depicted in Figure 2. PAH and SOF are polynuclear aromatic hydrocarbons and soluble organic fractions of PM, respectively, and make up part of the PM composition in the engine exhaust. A very important piece of information about the DOC missing from Figure 2 is the NO oxidation capability of the DOC. Furthermore, the excess air condition results in a lower engine operating temperature relative to a gasoline engine. As will be described below, NO oxidation is kinetically challenging under normal diesel exhaust temperature conditions.

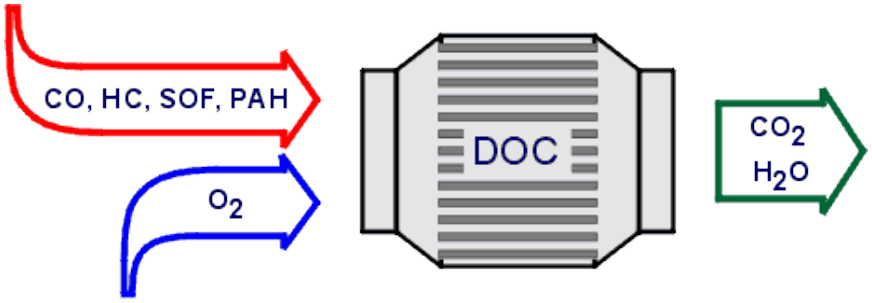

Figure 2: Conversion of pollutants on a diesel oxidation catalyst [11].

The main focus of this thesis is the investigation of the reactions involving NO_x and HC species that occur over the DOC. In much of the literature, the focus has been on the separate oxidation of HC and NO oxidation. The limited literature that does exist demonstrates that NO, CO and HC oxidation over a platinum (Pt) supported on alumina (Al_2O_3) catalyst, a typical example of a DOC, mutually inhibit one another due to competitive adsorption over the active sites. Also, the reaction between NO_2 and HC/CO occurs where NO_2 oxidizes the HC or CO and reverts back to NO, so NO oxidation is inhibited until HC and CO oxidation is complete [12]. However, another possible route can be proposed where the HC would react with the surface NO_x species: nitrites and nitrates. This reaction route is suggested because an enhancement in soot oxidation has been linked to surface nitrates/nitrites [13]. This surface reaction route has not been studied extensively thus far; therefore, a qualitative (IR spectroscopy) and quantitative (reaction kinetics) study of this system forms the basis of this thesis.

Chapter 2
Literature Review

This literature review covers DOC fundamentals and the reactions that occur over the catalyst, and mainly focuses on reactions involving NO_x and unburned HCs in the presence of O_2.

2.1 Diesel Oxidation Catalyst

DOCs are part of the diesel engine exhaust gas aftertreatment system. They commonly consist of precious metals, such as Pt, palladium (Pd) and/or rhodium (Rh) supported on high surface area materials like Al_2O_3. The Pt and Pd components are excellent oxidation catalysts and are used, as mentioned in Chapter 1, to oxidize CO, HC and NO. The DOC is quite effective in the oxidation of CO and HC to CO_2 and H_2O; however, the same cannot be said for NO. Note: when NO is oxidized to NO_2, the net NO_x output is not reduced.

The operating condition of the diesel engine is lean (O_2-rich), which makes reduction of NO_x to N_2 challenging [14]. The lean operating condition also causes the operating and therefore exhaust gas temperature to be lower than those of gasoline engines, which is also why a DOC is used upstream of other catalyst components, because the exotherm generated during CO and HC oxidation can raise the exhaust temperature to the desired range. Since DOCs cannot reduce NO_x emissions, another component, a NO_x abatement system, is required. NO_x abatement systems can include selective catalytic reduction (SCR) catalysts and NO_x

adsorbers (traps) or a combination of the two. The NO_x abatement systems, which are summarized in Table I, actually utilize the higher NO_2 output leaving the DOC. The table also includes soot filters, which operate better with higher levels of NO_2 to oxidize any trapped soot [15].

Table I: NO_x abatement systems and their reactions.

Catalyst	**Reaction type**	**Emissions**
Selective catalytic reduction (SCR)	SCR by ammonia/urea: $4NO + 4NH_3 + O_2 \rightarrow 4N_2 + 6H_2O$ (slow) $2NO + 2NO_2 + 4NH_3 \rightarrow 4N_2 + 6H_2O$ (fast)	NO_x
NO_x adsorbers (traps)	NO_x adsorption - lean exhaust, reduction - rich conditions: $NO + 0.5O_2 \leftrightarrow NO_2$ $BaO + 2NO_2 + 0.5O_2 \rightarrow Ba(NO_3)_2$	NO_x CO HCs
Soot filters	Oxidation: $C + 0.5O_2 \rightarrow CO$ (~550℃) $NO_2 + C \rightarrow CO + NO$ (~300℃) $CO + 0.5O_2 \rightarrow CO_2$	PM

Since the engine out stream generally has a very high NO to NO_2 ratio, a DOC is placed upstream of the NO_x abatement systems for the higher NO_2 level needed for them to function more efficiently.

The current diesel oxidation catalyst structure is a ceramic (cordierite) or metal honeycomb monolithic substrate. This is a common structure used for most catalytic converters for vehicle emission control. Figure 3 shows the schematic of a catalytic converter.

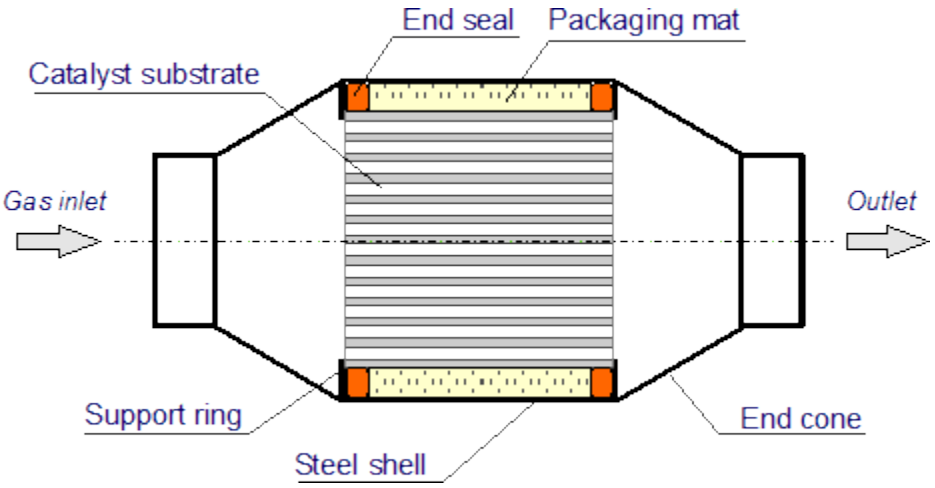

Figure 3: Schematic of a catalytic converter [16].

Catalyst monoliths are wrapped in a packaging mat and canned into a steel shell. The cordierite honeycomb structure invented by Corning provides thermal and mechanical shock resistance with a high melting point temperature of about 1450°C [3]. Metal supports are also sometimes used, resulting in decreased pressure drop due to thinner walls and also have better thermal conductivity properties [9]. The design flexibility of the honeycomb structure allows optimization of both geometric and physical properties of the substrate, which improve the overall physical strength of the catalytic converter system and make it possible to withstand stress under real applications. However, the cordierite or metal monoliths do not have high surface areas and porosities so it does not make sense to disperse the noble metal catalysts on them directly. Instead, a high surface area material, called the washcoat, is deposited on the substrate, and the metal catalysts are dispersed typically through impregnation. An example is shown in Figure 4.

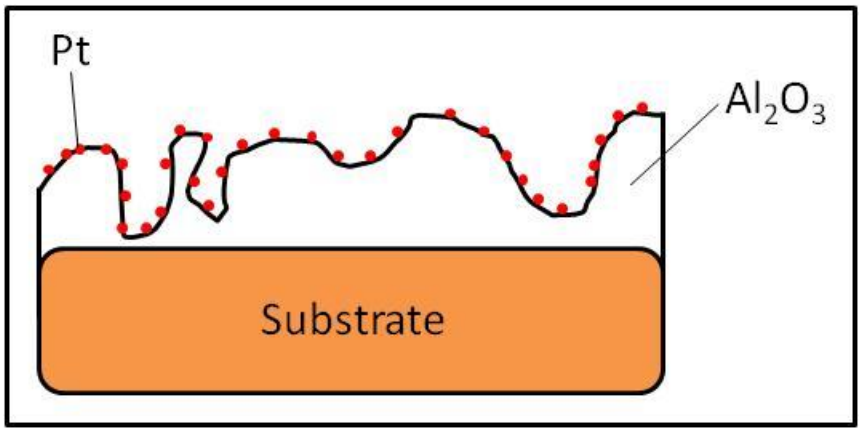

Figure 4: Example of precious metal catalyst (Pt) dispersed on a washcoat (Al_2O_3) adhered on a substrate.

Washcoat adhesion to the monolith is a key step in catalyst preparation because in real applications it is subjected to high gas flow rates and significant temperature gradients [3]. As mentioned before, Pt and Al_2O_3 are the common choices for precious metal and washcoat components for DOCs. Other washcoats or support materials are silica (SiO_2), zeolites and different combinations of these choices can be used as well [17]. Each precious metal and support has its own strengths and weaknesses. For example, Rh has better thermal stability than the other metals but it is not economical to use only Rh, while Pt and Pd often prove to be better oxidation catalysts. Zeolites have the ability to adsorb HCs, which could be beneficial for cold start periods since during this period the catalyst temperature is too low to oxidize these species [18]. However, zeolite-based DOCs can be deactivated at high temperatures especially in moist conditions [19] and are also susceptible to chemical deactivation due to fuel impurities [20]. Pd-based catalysts are more economical than Pt-based ones and Pd is also more thermally stable than Pt [21], but it is more susceptible to sulfur poisoning [22]. All these different factors are considered and utilized to optimize and

design the catalyst. Since diesel engines operate at lower temperatures than gasoline engines, DOCs generally require two to three times more precious metal than TWCs to achieve the same level of pollutant removal. Pt is the most common choice since it has the highest oxidation activity at low temperatures [23], a lower relative surface oxygen coverage, with high coverages detrimental by blocking active sites, and is better at oxidizing heavier HCs than other metals [17].

Current commercial catalysts utilize uniform distribution of precious metal loading over the length of the monolith. Recent modeling studies have predicted that zone-coated catalysts (non-uniform distribution) would enhance catalytic converter performance. A study by Kim et al. [24] focused on optimizing a non-uniform distribution of metal catalyst to reduce pollutant emissions. The results showed that by having more catalyst at the front and less at the back, improved light off performance and lowered overall CO, HC and NO emissions could be attained. Other modeling studies show the same prediction that a front-loaded catalyst will reduce the pollutant emissions more effectively [25–26]. However, this distribution can be problematic since it can lead to thermal deactivation and can affect the catalyst inlet more significantly [27], although other studies suggest the back is more affected [28]. Catalyst activity decreases via catalyst agglomeration when subjected to high temperatures.

2.1.1 Deactivation

In catalytic converters, two major types of deactivation occur: physical (sintering) and chemical (poisoning) [29]. Thermal deactivation generally refers to sintering and it is when the surface area decreases due to structural changes. It can occur to both the precious metal and the support [21–22,29]. The main source of poisoning is sulfur, which originates from the fuel or oil, and is oxidized during combustion to SO_x. Other sources of catalyst poisoning originate from fuel impurities and lubricants [9]. Figure 5 illustrates the two deactivation mechanisms: sintering and poisoning.

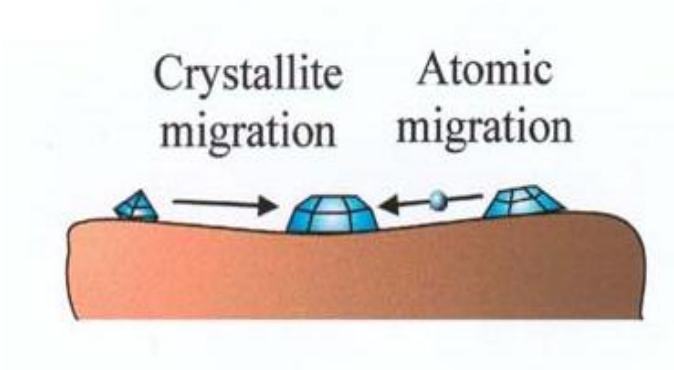

(a) Sintering

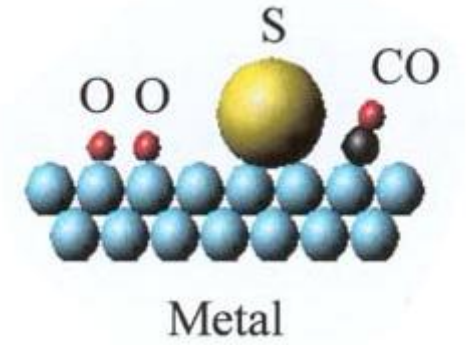

(b) Poisoning

Figure 5: Catalyst deactivation via (a) sintering and (b) poisoning [30].

Thermal deactivation can change the Al_2O_3 support morphology. The highest surface area (desired) form is γ-Al_2O_3. During support sintering, the pores become smaller or blocked off, which can effectively trap and seal in precious metal components so that reactants can no longer reach them and the catalytic activity decreases [29]. Sintering can also affect the precious metal itself so that it becomes mobile at higher temperatures and agglomerates with other metal particles. When the particle size increases through agglomeration, it decreases the active area exposed per volume and the catalytic activity.

Poisoning deactivation occurs via undesired chemisorption of species on the active metal or the support. While sintering causes permanent damage to the catalyst, poisoning can be either temporary or permanent. Sulfur poisoning can sometimes be reversible since the sulfur species may desorb above 500℃ [17] or irreversible especially when the support morphology is affected.

A more extensive review of the DOC written by Russell and Epling [17] is available in *Catalysis Reviews*.

2.2 NO Oxidation

In diesel exhaust, NO_x is composed of mainly NO. Since NO_x adsorbers and selective catalytic reduction (SCR) catalysts are more efficient with higher levels of NO_2, a DOC is generally the first catalyst used in a diesel exhaust aftertreatment system to convert NO to NO_2 as well as oxidize the CO and HC species. Pt is an excellent NO oxidation catalyst,

while other precious metals, such as Rh and Pd are not as effective [31]. NO oxidation is an exothermic and equilibrium-limited reaction within the higher temperature range of diesel exhaust: $NO_{(g)} + ½\ O_{2(g)} \leftrightarrow NO_{2(g)}$. The NO oxidation reaction is also limited by kinetics at low temperature, at least relative to CO and HC oxidation. For Pt supported on Al_2O_3 (Pt/Al_2O_3) catalysts, equilibrium is reached in typical exhaust compositions at about 350°C, as reported by Olsson et al [32] as shown in Figure 6.

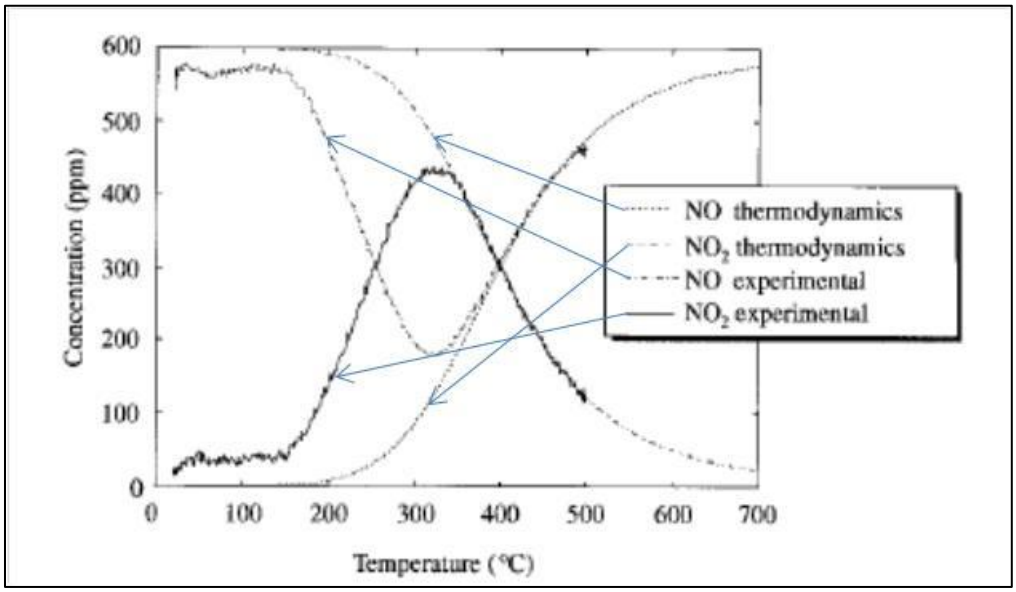

Figure 6: Concentrations of NO and NO_2 during a temperature-programmed oxidation experiment, with 600 ppm NO and 8% O_2 in Argon (Ar) [32].

NO oxidation kinetics are affected by Pt loading, dispersion and support material. For NO oxidation, Xue et al. [33] suggested it operates according to the Langmuir-Hinshelwood mechanism, where NO sorbs on the support and migrates to Pt particles, oxidizes to NO_2 and then desorbs. Olsson et al. [34] also found the Langmuir-Hinshelwood model to be most

probable for NO oxidation over Pt/Al_2O_3. NO oxidation kinetics over Pt/Al_2O_3 were also studied by Mulla et al. [35] who found that the reaction is first order in both NO and O_2 and nearly negative first order for NO_2. Westerberg and Fridell [36] observed that nitrites and nitrates readily formed on the surface when the catalyst was exposed to NO oxidation conditions. These surface NO_x species are thermally stable at temperatures < 300°C. However on a SiO_2 support, which is relatively inert, faster reaction rates are achieved since the formed NO_2 desorbs easily [33]. Surface reactions will be further discussed in section 2.5. Xue et al. also reported an increase in NO oxidation activity with an increase in Pt loading but it was unclear whether the improved performance was directly related to Pt loading.

Several studies have shown that NO oxidation improves with increasing particle size [33,37–38] to a certain point before decreasing. Particle sizes increase with sintering as the Pt particles migrate and agglomerate, leading to a decrease in the exposed active area. So whatever the reason for the positive effect of increasing particle size is, a limit is reached when the active area becomes too small. Denton et al. [37] reported that the activity was still increasing with particle size at a dispersion as low as 2.6%. Olsson and Fridell [38] explained that with small particle sizes (large dispersion), more Pt oxides or more chemisorbed oxygen on the Pt are formed. The product NO_2 from NO oxidation is also a strong oxidant and can also increase the surface oxygen coverage. Parker et al. [39] showed that when Pt was exposed to NO_2, it produced a high coverage of adsorbed oxygen atoms on the Pt surface. As mentioned earlier, surface oxygen coverage can block active sites for oxidation reactions and decrease activity and Pt oxides are less active than metallic Pt. Thus NO oxidation is

inhibited by its own product NO_2. The smaller Pt particles are more easily oxidized and the oxide species are more stable relative to those on larger particles, requiring higher temperatures for the oxygen to desorb and thus lower NO oxidation rates.

2.3 Hydrocarbon Oxidation

Diesel engine exhaust contains a complex mixture of unburned HCs, including aromatics, unsaturated (alkenes and alkynes) and saturated (alkanes) HCs. Generally, for experimental studies, propane (C_3H_8) is used for saturated HCs and propylene (C_3H_6) is used for unsaturated HCs [40]. Voltz et al. [41] reported the activation energy of C_3H_6 oxidation over Pt/Al_2O_3 to be 120.97 kJ/mol. However, diesel engine exhaust also contains NO_x, CO and other pollutants. When all these pollutants are present, they can affect the oxidation of each other over the DOC. When more than one HC is present, they compete for active adsorption sites and the HCs that adsorb most strongly to the active sites are oxidized first. Mittendorfer et al. [42] reported that for aromatics, adsorption to Pt and Pd is dominated by the interaction between the aromatic ring with the surface and they are generally more weakly adsorbed compared to other HCs. Mabilon et al. [43] found most unsaturated HCs adsorb strongly when CO was present and oxidized at below the light off temperature for CO oxidation. They found that acetylene had the strongest inhibition effect of all unsaturated HCs they tested and it determined the light-off temperature of other compounds. They also observed an increase in adsorption strength with molecular size, but other factors play a role based on their findings. For example, Mittendorfer et al. [42] also looked into the adsorption of olefins and compared 1-butene (C_4H_8) and ethylene (C_2H_4). They observed the adsorption of C_4H_8 to be

significantly weaker in terms of adsorption energy, thus showing that it cannot be explained by molecular size only. The interactions also involve the energy associated with the deformation of the molecules and the surface during adsorption [42].

Similar to NO oxidation over Pt/Al_2O_3, an increase in Pt particle size appears to improve HC oxidation as well. This was seen by Benard et al. [44] and Denton et al. [45], who observed that the Pt-O bond strength is smaller for larger particles, favoring the adsorption of other species and leading to increased total HC oxidation. The same increased activity was seen in an earlier study by Briot et al. [46] in which they studied methane oxidation over Pt/Al_2O_3.

Grbic et al. [47] tested the oxidation of a binary mixture of HCs, toluene and n-hexane, over Pt/Al_2O_3 with varying metal dispersions and found that n-hexane could be more strongly bound than toluene to smaller Pt particles and vice versa for larger particles. However, while more n-hexane was adsorbed to the smaller Pt particles than toluene, toluene was still more reactive due to its weaker C–H bonds. This indicates adsorption strength is not the only factor as HC reactivity is also determined by the strength of the C–H bond.

2.4 NO_x and Hydrocarbon Interactions

An important area of study is the interaction of NO_x and HCs on the DOC surface since diesel exhaust contains both pollutants among others. A study by Voltz et al. [41] showed that in a mixture of NO, CO and C_3H_6, oxidation of each over Pt/Al_2O_3 was inhibited by the others. This inhibition effect increased with increasing concentrations of each gas. Irani et al.

[12] also observed similar trends in temperature-programmed oxidation experiments over a Pt-Pd/Al_2O_3 sample with NO, C_3H_6 and O_2. Data clearly showed a strong inhibition of NO oxidation in the presence of C_3H_6 and vice versa. The concentration of C_3H_6 was varied from 100 to 1000 ppm and the inhibition effect on NO oxidation increased with C_3H_6 concentration. The inhibition effects are displayed in Figure 7.

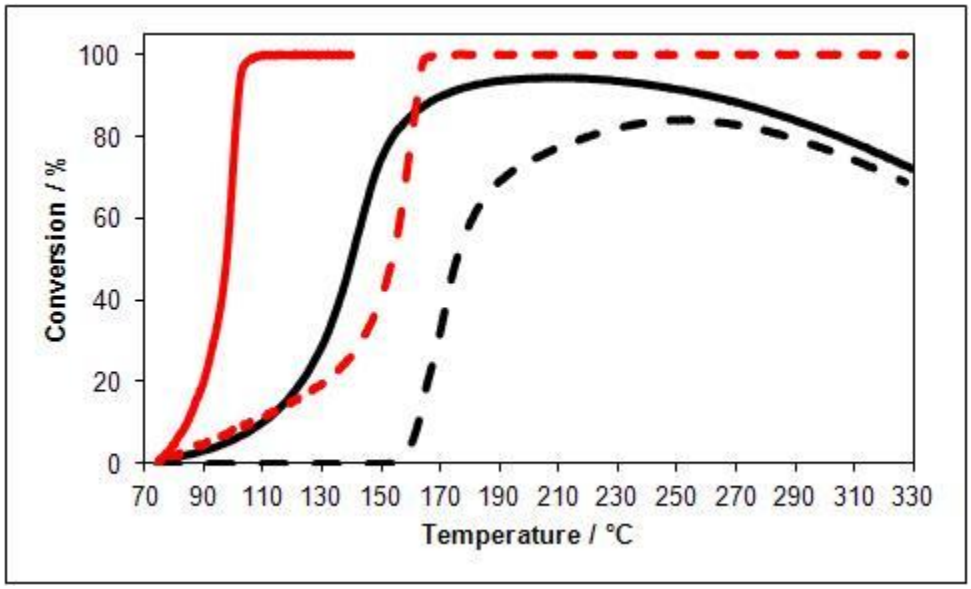

Figure 7: Example conversion profiles of NO and C_3H_6 during temperature-programmed oxidation over Pt/Al_2O_3 individually (—: NO and —: C_3H_6) and in the presence of one another (--- and ---). Feed gas composition: 250 ppm NO and/or 200 ppm C_3H_6, 6.5% O_2, 5% H_2O and balance N_2.

Although the inhibition of C_3H_6 oxidation by NO is mainly due to competition for adsorption sites, that was not the only reason for NO oxidation inhibition by C_3H_6. While NO oxidation may have been occurring, NO_2 was not observed until most of C_3H_6 was oxidized. This

suggests that NO_2 was being consumed as a reactant, acting as an oxidant for C_3H_6 oxidation. Furthermore, NO_2 was preferentially consumed relative to O_2. Although NO_2 promotes C_3H_6 oxidation, as more NO forms with increasing temperature, the inhibition effect takes over. A similar trend was observed in a study by Al-Harbi et al. [48].

2.5 NO_x and Hydrocarbon Surface Reactions

As mentioned earlier, NO and NO_2 in the presence of O_2 adsorb quite readily on a Pt/Al_2O_3 catalyst surface, forming nitrites and nitrates, as has been well studied by many researchers [36, 49–51]. Westerberg and Fridell [36] reported that Al_2O_3 was found to be an important storage site for adsorbed NO_x species at temperatures below 300°C. In a study by Castoldi et al. [15], it was suggested that for some catalyst types, the formation of these surface NO_x species is one of the most important reasons for enhanced soot oxidation performance. An increase in soot oxidation activity in the presence of NO and O_2 was observed by Pieta et al. [52] as well.

Haneda et al. [53] studied HC oxidation over a Pt/Al_2O_3 catalyst using IR spectroscopy. Using a HC mixture of n-decane and 1-methylnaphthalene, they found carbonate and/or carboxylate species on the surface. It is difficult to accurately assign the corresponding species for HC adsorption as there are many overlapping peaks for HC adsorption in the IR spectra. From their transient analysis, Haneda et al. were able to identify some intermediate species formed, such as acrylates, which were formed first and then consumed as CO_2 formed. It is therefore apparent that Al_2O_3 is also an important site for adsorbed HC species.

Anderson and Rochester [54] studied C_3H_6 oxidation over a Rh/Al_2O_3 catalyst and also observed the formation of carboxylates, carbonates and acrylates on the surface.

Chapter 3
Experimental Methods

To investigate the interaction between NO_x and HC on a DOC, various experiments were performed. This chapter introduces the different instruments and procedures used in this thesis work.

3.1 Apparatus and Experiment Techniques

A pilot scale plug flow reactor (PFR) was used for experiments with monolith samples of 1 inch diameter and 2 to 3 inches in length that were wrapped in high temperature 3M matting material and inserted into a quartz tube reactor. The purpose of the 3M matting material is to prevent any gas bypass between the quartz tube wall and the wall of the monolith sample.

A Lindberg/Blue Mini-Mite tube furnace was used to heat the reactor. The feed gases were metered with Bronkhorst mass flow controllers before entering the reactor. The tubing leading up to the reactor was heated to above 100℃ to prevent H_2O condensation. All gases were supplied by PraxAir except N_2, which was generated with a system manufactured by OnSite Gas Systems. Water was added using a Bronkhorst CEM system. Three K-type thermocouples were placed in the upstream, front, and the back of the monolith sample for temperature measurements. Photographs of the pilot reactor with the monolith sample inserted are shown in Figure 8.

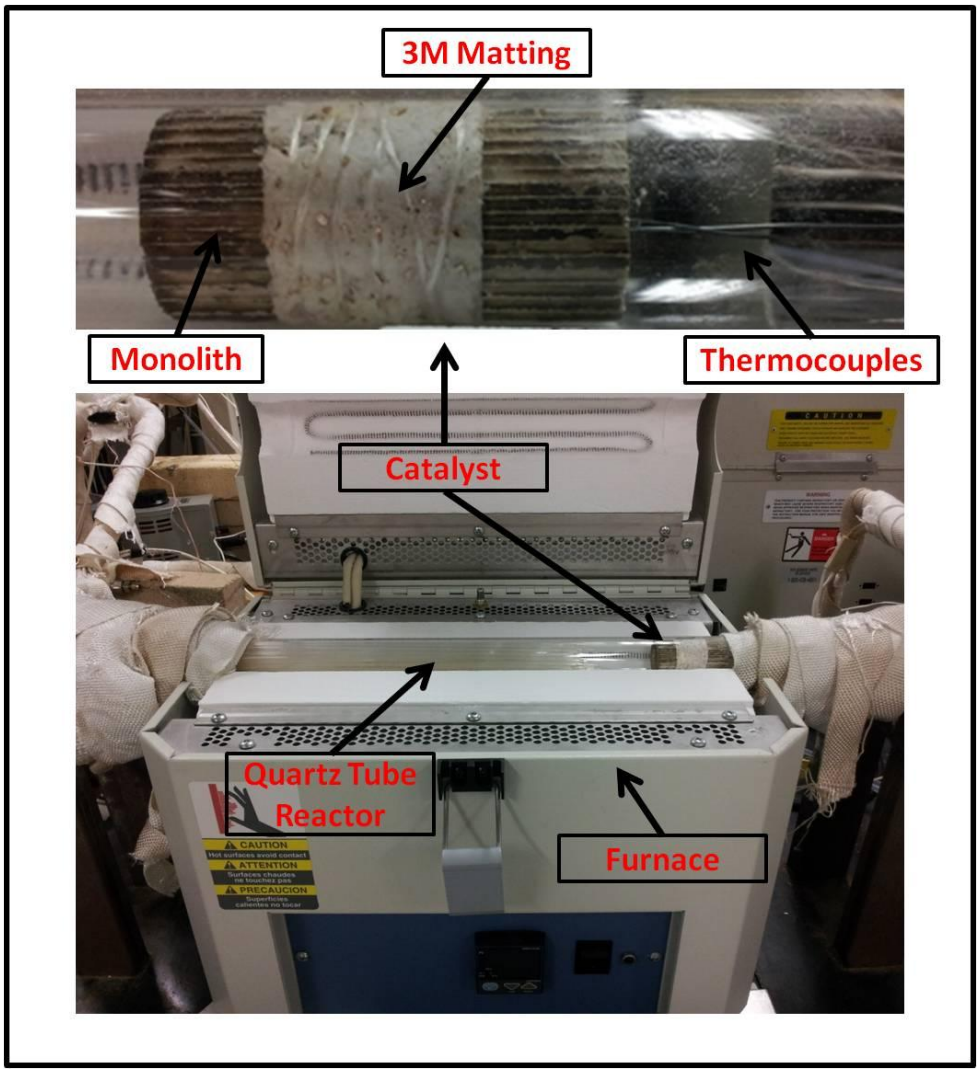

Figure 8: Monolith sample with thermocouples attached inside a quartz tube reactor.

The system contains two gas manifolds so that different gas mixtures can be prepared, but only one of these is introduced to the reactor at a time while the other is sent to exhaust ventilation. A LabView program controls the type and amount of gas flowing in each gas manifold and the gas flowing to the reactor. A 4-way actuated switching valve, powered with compressed N_2, is used to direct the two flows. The LabView program also records the temperature of the various thermocouples in the reactor over time. The outlet gas stream is

analyzed using a MKS 2030 FTIR MultiGas analyzer. The MKS FTIR has calibration files provided by the manufacturer that convert the IR spectra recorded to species concentrations, in either ppm or percent, versus time. Various types of experiments can be performed using this pilot reactor. This includes temperature-programmed oxidation (TPO), where the temperature is ramped at a specified rate to measure its effect on the oxidation reaction or steady state experiments where isothermal inlet conditions are set. Similar to TPO, temperature-programmed desorption (TPD) experiments can be performed to observe what species desorb from the catalyst during a temperature ramp. By using LabView to control the programmed switching function of the two gas manifolds, specific gas mixtures can be "pulsed" into the reactor in this mode; this type of experiment will be referred to as a pulse experiment for the rest of this thesis.

Powder samples were used for the Hiden CATLAB Micro-reactor and the Diffuse Reflectance Infrared Fourier Transform Spectroscopy (DRIFTS) experiments, which were analyzed in a Thermo Nicolet 470 FT-IR Spectrometer equipped with a MCT detector. 1 wt-% Pt/γ-Al_2O_3 powder (300 m^2/g) and Al_2O_3 powder (γ-phase) purchased from Alfa Aesar were used for the powder sample studies. 50 mg of sample catalyst particles (40-60 mesh) were loaded into the quartz-tube CATLAB Micro-reactor. The outlet gas stream was analyzed using a Hiden QIC-20 mass spectrometer (MS-based) or a Pfeiffer Vacuum OmniStar Gas Analysis System (also MS-based) and calibrated with reference gases. This analysis system will be referred to as CATLAB. For CATLAB, small but known amounts of Ar were always introduced as an inert gas, other than the carrier gas, so that any changes due to pressure sensitivity would be corrected by dividing MS measurements of other gas

concentrations by those of the Ar. The gas flow rate in the CATLAB studies was always 95 mL/min. The same types of experimental studies can be performed on the micro-reactor as those previously described for the pilot reactor (TPO, TPD, steady state and pulsing). The MS needs to be calibrated using the raw MS signal and those obtained with reference gases at different concentrations. This is done by flowing a known concentration of a specific gas to the MS and calibrating against the raw signal. TPO experiments reveal inhibition effects and also the oxidation reaction kinetic parameters can be calculated from TPO data. TPD experiments can often be used to quantify how much adsorption occurred on the surface.

For experiments done with the FT-IR Spectrometer, with diffuse reflectance infra-red Fourier transform spectroscopy used, IR spectra can be obtained, and these are used to determine what species are adsorbing/desorbing to/from the catalyst when exposed to the specified gas mixture and temperatures. The sample catalyst was exposed to NO_x and HC in different sequences or together to characterize the surface interactions. DRIFTS spectra were used for qualitative studies and the data obtained show peaks at certain wavelengths that represent different species. An example DRIFTS spectrum is shown in Figure 9.

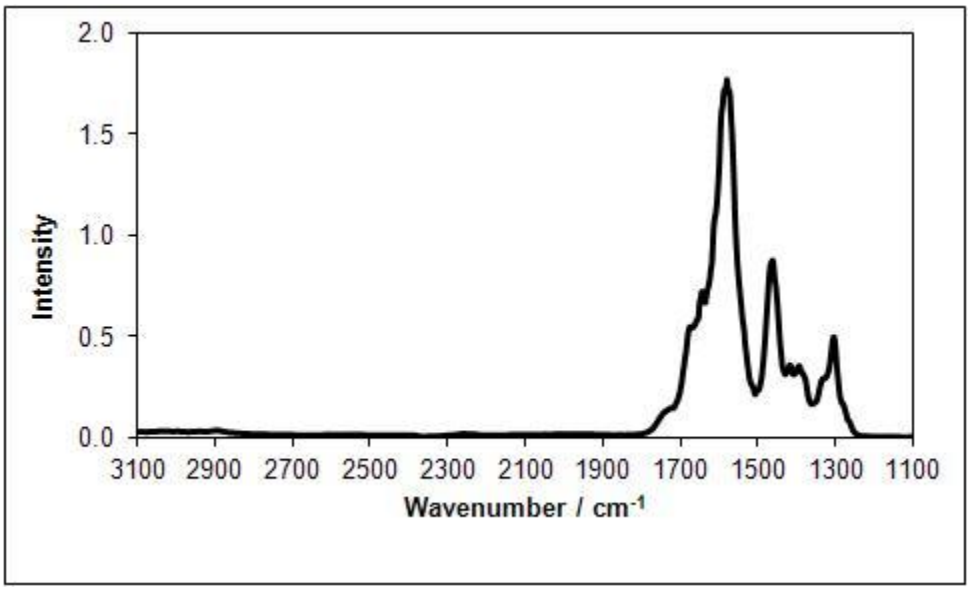

Figure 9: A sample IR spectrum showing the intensities of different peaks at specific wavenumbers that represent different species formed on the surface.

The challenge in analyzing DRIFTS data is to correctly identify the species corresponding to each peak through comparison with those available in the literature, i.e. finding literature results that correlate peak position and shape to the surface species present, typically through more fundamental study.

3.2 Experimental Procedure

3.2.1 NO Oxidation Inhibition by HCs over a DOC – Reaction Between Surface Nitrates and HCs

The reaction between NO_x and C_3H_6 was also investigated in the pilot reactor system. This was done using a monolith catalyst sample with an Al_2O_3 loading of 1.59 g/in^3 and a Pt

loading of 27.5 g/ft^3. The catalyst sample was 1 inch in diameter and 3 inches in length. A gas flow rate of 10 L/min was used, which corresponds to a space velocity of 25,000 hr^{-1}. C_3H_6 oxidation and NO oxidation, separately, were evaluated via TPO. Another TPO experiment was performed with both C_3H_6 and NO present. The temperature was ramped from 80℃ to 400℃ at a rate of 5℃/min. The feed gas compositions were 200 ppm NO and/or 1000 ppm C_3H_6, 5% O_2, 5% H_2O, 5% CO_2 with the balance being N_2.

The reactivity between C_3H_6 and stored nitrites/nitrates was also investigated using CATLAB on a 1 wt-% Pt/γ-Al_2O_3 powder. The outlet gas stream was measured by a Hiden QIC-20 mass spectrometer. For experiments done on CATLAB, the sample was cleaned by heating in 10% O_2, 0.1% Ar in a He balance for 90 minutes at 500℃. After cooling down to 250℃, 500 ppm NO, 10% O_2, 0.1% Ar in a He balance were introduced for 2 hours to store NO_x species on the catalyst. Then, temperature-programmed desorption (TPD) was performed from 250℃ to 500℃ at a heating rate of 10℃/min. The same experiment was also performed except that the catalyst was exposed to 50 ppm C_3H_6 for 3h after NO_x adsorption. Therefore, the amount of NO_x remaining on the surface before and after C_3H_6 exposure could be quantitatively analyzed.

For DRIFTS experiments, the catalyst was pretreated with 40 mL/min of He at 500℃ for 30 minutes, followed by 5% O_2 in He for 30 minutes and then 5% H_2 in He for another 30 minutes. For each spectrum, 45 scans were collected at a resolution of 4 cm^{-1}. The spectra were recorded in the 650 to 4000 cm^{-1} range. Bronkhorst mass flow controllers were used to set the feed gas concentrations and flow rates. A total gas flow rate of 40 mL/min was used

for all the experiments. Different sequences of C_3H_6 and NO exposure were evaluated. To characterize the interaction between gas-phase C_3H_6 and surface nitrates, first, 250 ppm NO, 5% O_2 and balance He were first introduced at 250℃ for 120 minutes in order to form surface nitrites/nitrates; afterwards, 200 ppm C_3H_6, 5% O_2 and balance He were introduced to investigate the reaction between C_3H_6 and nitrates. By replacing NO with NO_2, a similar experiment was performed as well. Experiments were also performed where the catalyst was exposed to C_3H_6 and O_2 first followed by NO_x and where NO_x and C_3H_6 were introduced together were also done.

3.2.2 Reaction Kinetics of C_3H_6 Oxidation for Various Reaction Pathways

The different pathways of C_3H_6 oxidation were investigated in the CATLAB by analyzing the outlet gas with a Pfeiffer Vacuum OmniStar Gas Analysis System. C_3H_6 oxidation via O_2, NO_2 and nitrates were studied over 1 wt-% Pt/Al_2O_3 and 1 wt-% Pt/SiO_2 powder samples. The Pt/SiO_2 catalyst sample used was made in the laboratory. In order to more directly compare the two catalysts a similar Pt dispersion was desired. H_2 chemisorption was performed on both catalysts to determine the Pt dispersion. Chemisorption experiments were done in CATLAB at a flow rate of 50 mL/min. For Pt/SiO_2, the catalyst was heated to 450℃ in 5% H_2 in He for 30 minutes and cooled down to 40°C in pure He. 100 µL of 5% H_2 in He were pulsed into the 50 mL/min of He flow every 30 seconds over a total of 26 cycles. For Pt/Al_2O_3, the catalyst was heated to 500℃ in 5% H_2 in He for 30 minutes and then the same procedure as above was used. The Pt/Al_2O_3 sample was then thermally aged at 650℃ in 5% H_2 in He for 2 hours and then exposed to 6.5% O_2 in He for 15 minutes followed by exposure

to 5% H_2 in He for another 15 minutes. These 15 minute exposures were repeated twice (total duration at 650℃ was 3 hours). The sample was then cooled down to 40℃ in He followed by H_2 chemisorption over 17 pulse cycles. Pt dispersions of Pt/SiO_2, Pt/Al_2O_3 and aged Pt/Al_2O_3 catalyst samples were 1.6, 23.1 and 1.3%, respectively.

Following the chemisorption tests, the reactivities of C_3H_6 with O_2 and then with NO_2 were investigated with CATLAB. TPO experiments were performed on the Pt/SiO_2 sample and the aged Pt/Al_2O_3 sample using 100 ppm C_3H_6, 6.5% O_2 and balance He as the feed gas at a flow rate of 95 mL/min. The temperature was ramped from 70℃ to 300℃ at a rate of 5℃/min. With the same feed gas composition, a similar experiment was done but in steps, where the temperature was held at a specific level until steady state was reached (constant conversion). Overall, the temperature was varied from 70 to 150℃, generally in 5℃ intervals. This will be referred to as the steady state ramp for this thesis. Step intervals of 5℃ were used because it was difficult to accurately measure the change in C_3H_6 concentration for anything less than a 5℃ change. The TPO and steady state ramp experiments were repeated with 1000 ppm NO_2 instead of 6.5% O_2. Prior to each of these experiments, the catalyst was pre-treated to 450℃ for Pt/SiO_2 and 500℃ for Pt/Al_2O_3 in He and then switched in exposure to 6.5% O_2 and 5% H_2 in He 10 times in 1 minute intervals. Each experiment was repeated at least once for reproducibility.

Lastly, to characterize the reactivity between nitrates and C_3H_6, the Pt/Al_2O_3 sample (fresh 1 wt-% standard) was tested under the assumption that no nitrates can form on SiO_2 (which was proven, details follow). The same pre-treatment, switching between 6.5% O_2 and 5% H_2

in He at 500℃, was done prior to this experiment. Following the pre-treatment, the sample was cooled down to 275℃ and then 1000 ppm NO_2, 6.5% O_2 and balance He was flown over the catalyst for 2 hours. After 2 hours, the sample was cooled in 6.5% O_2 in He for 15 minutes and then cooled to 70℃ in pure He. 100 ppm C_3H_6 in He was then added and the temperature was ramped to 350℃ at 1℃/min. This experiment was also repeated with 100 ppm C_3H_6 and 6.5% O_2 in He, with pure He and with 6.5% O_2 in He for the temperature ramp.

Chapter 4
NO Oxidation Inhibition by HCs over a DOC – Reaction Between Surface Nitrates and HCs*

**This chapter is reproduced from H. Oh, J. Luo, W. Epling, Catal Lett 141 (2011) 1746. DOI: 10.1007/s10562-011-0714-z.*

4.1 Results and Discussion

As reported in the literature, NO oxidation inhibits C_3H_6 oxidation while the product NO_2 acts as an oxidant for C_3H_6 oxidation. However, when NO_2 reacts with C_3H_6, it produces NO, which leads to C_3H_6 oxidation inhibition. In the case of soot oxidation, NO_2 is a strong oxidant. For some catalyst types, the formation of nitrites/nitrates on the surface is proposed to be one of the most important reasons for enhanced soot oxidation performance [13]. Since adsorbed nitrites and nitrates have also been observed on Pt/Al_2O_3 catalysts with exposure to NO/NO_2 [36,49–51], these may account for some of the HC oxidation activity. In order to determine whether HCs can be oxidized by surface NO_x species, DRIFTS was used to characterize surface species that formed or were consumed before, during and after different sequences of NO_x and C_3H_6 exposures. The reaction between NO_x and C_3H_6 was also investigated in a pilot reactor system and CATLAB.

4.1.1 Pilot Reactor

C_3H_6 oxidation in the presence and absence of NO, and NO oxidation in the absence and presence of C_3H_6 were evaluated via TPO to yield the results displayed in Figure 10. C_3H_6 oxidation was negatively affected in the presence of NO in the feed stream as expected, with

the light-off temperature increased by around 60°C due to competitive adsorption of NO and C_3H_6 for Pt sites [12,41].

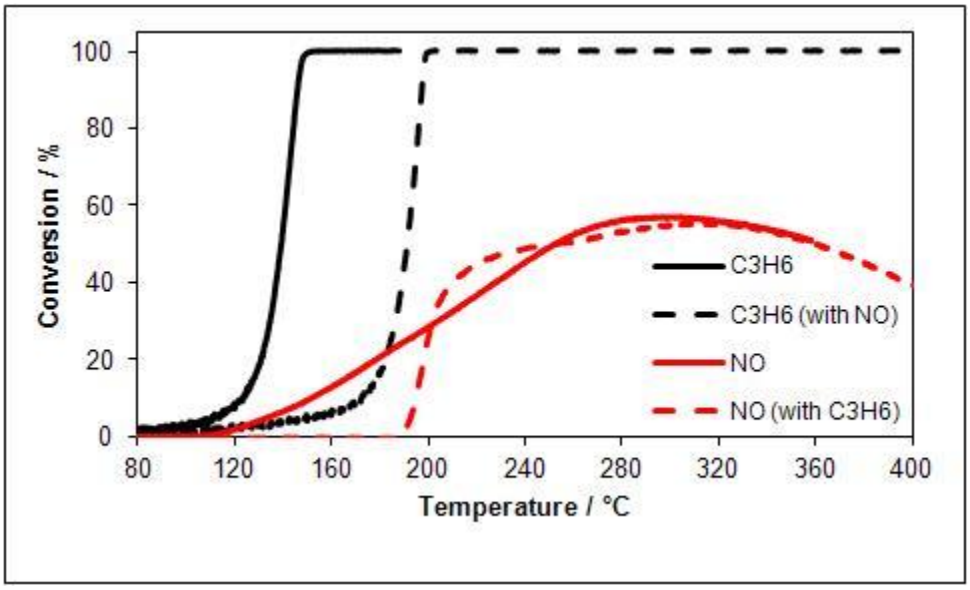

Figure 10: Conversion profiles of C_3H_6 and NO during temperature-programmed oxidation over Pt/Al_2O_3 individually (— and —) and in the presence of one another (--- and ---). Feed gas composition: 200 ppm NO, 1000 ppm C_3H_6, 5% O_2, 5% CO_2, 5% H_2O and balance N_2.

When the temperature was below 200°C, NO oxidation to NO_2 was negatively affected by the presence of C_3H_6, with NO_2 observed only once most of the C_3H_6 was oxidized, as any NO_2 formed can be consumed by C_3H_6 [12]. However, between 200 and 250°C, there was a slight improvement in NO conversion to NO_2 observed in the presence of C_3H_6 before being inhibited again between 250 and 320°C.

4.1.2 CATLAB and DRIFTS

As an initial demonstration of adsorbed nitrites/nitrates acting as reactants, TPD of NO_x from a Pt/Al_2O_3 powder surface first exposed to NO + O_2 was run and then compared with a TPD run where the sample was exposed to C_3H_6 after the NO + O_2 exposure in the CATLAB micro-reactor. The results are shown in Figure 11.

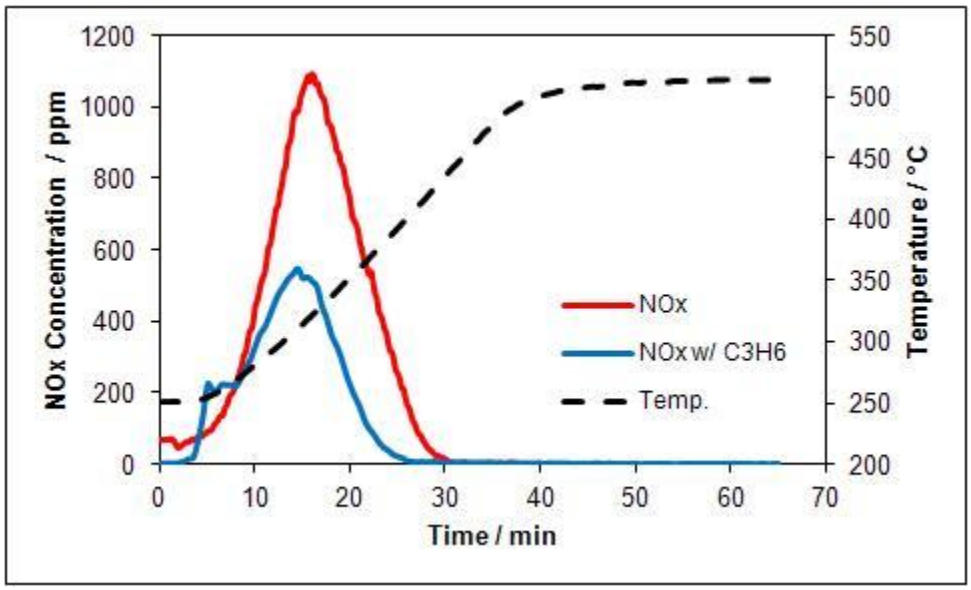

Figure 11: Concentration of NO_x released during temperature-programmed desorption over Pt/Al_2O_3 following NO oxidation (—) and then exposure to C_3H_6 (—)**.** Temperature ramp curve shown by ---. Feed gas composition: 500 ppm NO, 50 ppm C_3H_6, 10% O_2 and balance He.

Approximately 50.4% of the NO_x was left on the surface after C_3H_6 exposure, indicating that reaction can indeed occur between C_3H_6 and surface nitrates.

The DRIFTS spectra showing evidence of NO adsorption at 250℃ over 1 wt-% Pt/γ-Al_2O_3 as a function of time are shown in Figure 12.

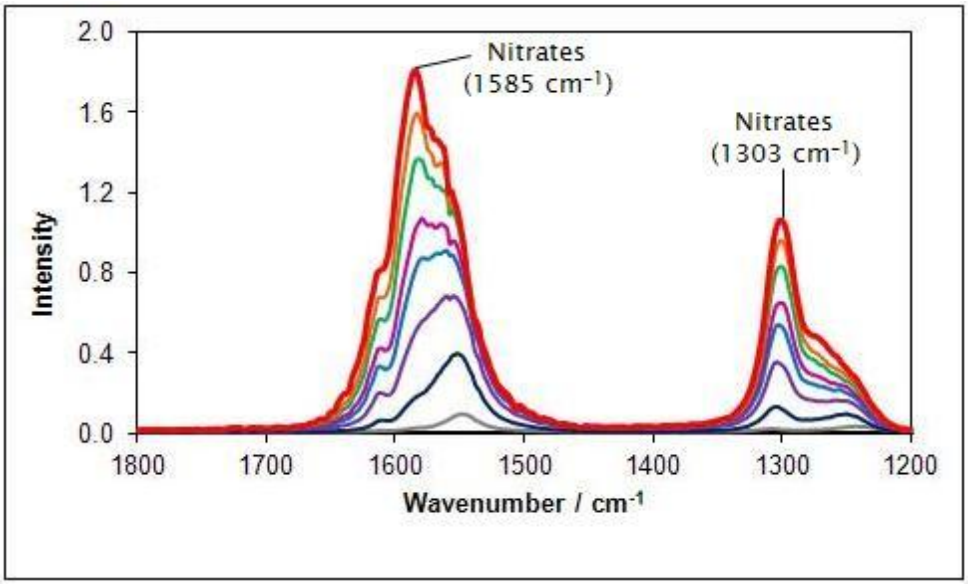

Figure 12: DRIFTS of 1 wt-% Pt/Al_2O_3 at 250℃ exposed to NO + O_2 for times 0, 5, 10, 20, 30, 35, 45, 55 and 120 min (black to red). Feed gas composition: 250 ppm NO, 5% O_2 and balance He.

Most of the peaks in the range from 1200 to 1800 cm^{-1} can be assigned to nitrates formed on the alumina surface. Specifically, overlapping bands in the 1500–1650 cm^{-1} and 1200–1350 cm^{-1} region can be attributed to monodentate, bidentate and bridged nitrates [36,49–51]. Within the first 5 minutes, bridging nitrite bands appear at 1233 and 1310 cm^{-1} and a low coverage nitrate band appeared at 1550 cm^{-1} along with a small shoulder at 1615 cm^{-1}. With the Pt/Al_2O_3 catalyst, nitrites are readily oxidized to form nitrates, which began to appear, at 1303 cm^{-1}, in the spectrum within 15 minutes of exposure. The peak intensities increased

with time until saturation was reached after about 75 minutes of exposure. The final peaks at 1585 and 1303 cm^{-1} are most likely monodentate nitrates with the 1615 cm^{-1} shoulder attributed to bidentate nitrates. Assigning each of these peaks to a specific type of nitrate is difficult due to the overlap and is not the specific focus of this paper, and so they will simply be considered as nitrites or nitrates, with emphasis being on what happens to these in the presence of C_3H_6 and O_2. The exact same peaks excluding formation of nitrites were observed in spectra obtained using NO_2 as the feed NO_x source.

Following NO_x adsorption, the catalyst was exposed to C_3H_6 and O_2 and the resulting DRIFTS spectra as a function of time are shown in Figure 13.

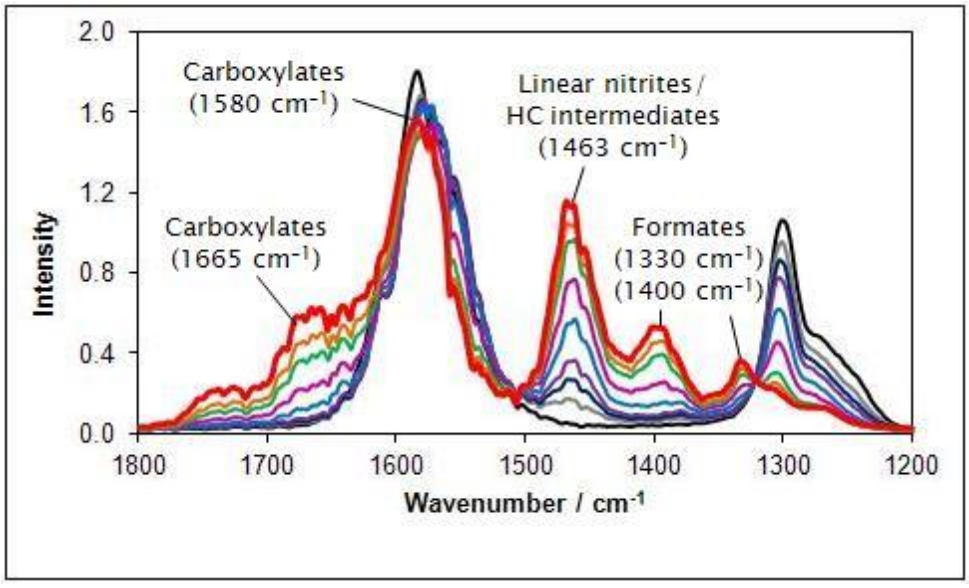

Figure 13: DRIFTS of 1 wt-% Pt/Al_2O_3 at 250℃ exposed to C_3H_6 + O_2 following NO adsorption for times 0, 5, 10, 15, 20, 35, 60, 95 and 170 min (black to red). Feed gas composition: 200 ppm C_3H_6, 5% O_2 and balance He.

With extended C_3H_6 exposure, the nitrate bands, such as that at 1303 cm^{-1}, decreased substantially. The bands around 1580 cm^{-1} decreased as well, but not as significantly as carboxylate species were formed simultaneously during C_3H_6 oxidation, and have bands at 1580 cm^{-1} (OCO symmetric stretching) that overlap with the nitrate features. At the same time, other bands at 1330 cm^{-1} (OCO asymmetric stretching) and 1400 cm^{-1} (C-H bending) indicate the formation of formate species [55–60]. It is worth noting that a peak at 1463 cm^{-1} was also observed. This peak can be attributed to the formation of either linear nitrites [59,61] resulting from the reduction of nitrates by C_3H_6 exposure or acetate and acrylate species [61–64] resulting from C_3H_6 oxidation. This feature will be discussed in detail below. The group of peaks at 1642, 1650, 1658, 1665 and 1672 cm^{-1}, on the shoulder of the 1580 cm^{-1} band, are associated with carboxylate groups (C=O stretch) [56,65]. The intensities of the newly formed bands increased until saturation was reached after around 130 minutes.

For comparison, C_3H_6 adsorption over a clean surface, without pre-adsorption of NO_x, was also evaluated and the results are shown in Figure 14.

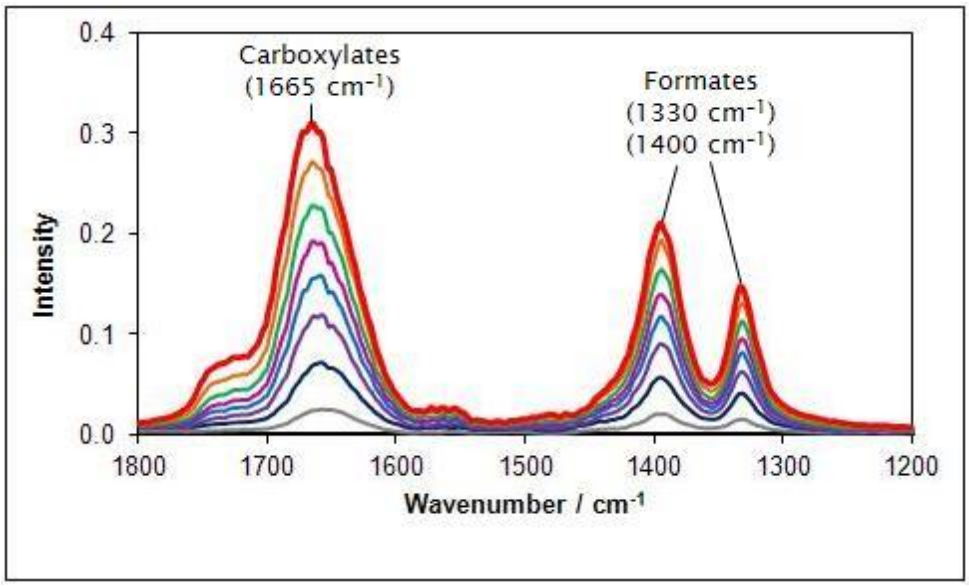

Figure 14: DRIFTS of 1 wt-% Pt/Al_2O_3 at 250℃ exposed to $C_3H_6 + O_2$ for times 0, 10, 30, 60, 90, 120, 160, 230 and 320 min (black to red). Feed gas composition: 200 ppm C_3H_6, 5% O_2 and balance He.

The intensities of the adsorption bands were much lower than when NO_x is present and the major bands at 1332, 1395 and 1665 cm^{-1} can be attributed to formate formation. All three of these peaks appeared at the same time and the intensities increased very slowly until reaching saturation after around 290 minutes.

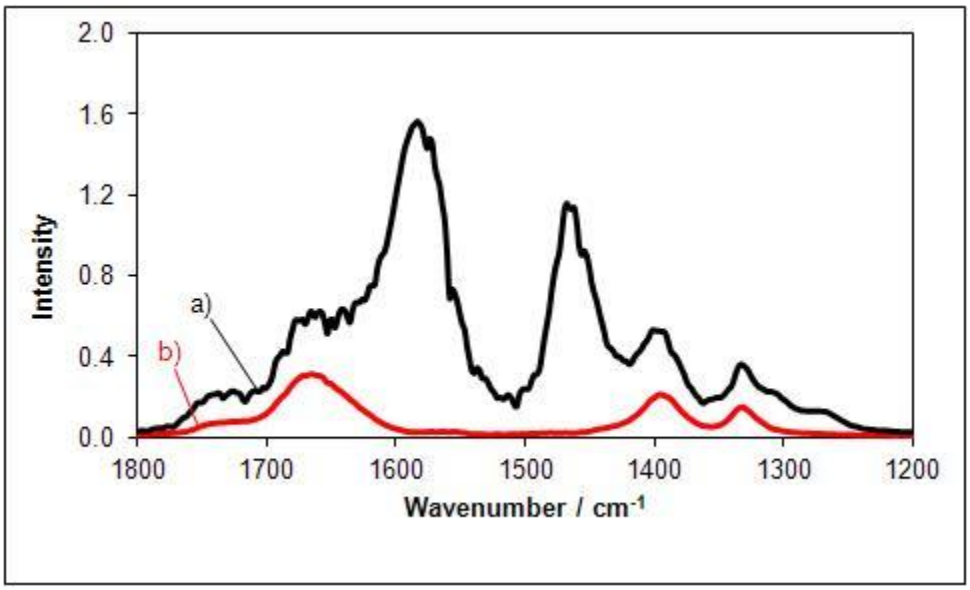

Figure 15: DRIFTS of 1 wt-% at 250℃ Pt/Al_2O_3 at 250℃ exposed to C_3H_6 + O_2 for 170 minutes after NO adsorption (a) and for 320 minutes on fresh catalyst (b). Feed gas composition: 200 ppm C_3H_6, 5% O_2 and balance He.

In Figure 15, the spectra collected after C_3H_6 oxidation (Fig. 14) in the absence of NO_x and after NO_x exposure followed by C_3H_6 oxidation (Fig. 13) are overlaid. This comparison demonstrates that the bands at about 1580 and 1463 cm^{-1} are directly related to the reaction between surface nitrates and C_3H_6 since they do not appear in the absence of NO_x.

When the catalyst was first exposed to C_3H_6 and O_2 in the absence of NO_x but then exposed to NO_2, the spectra shown in Figure 16 are obtained.

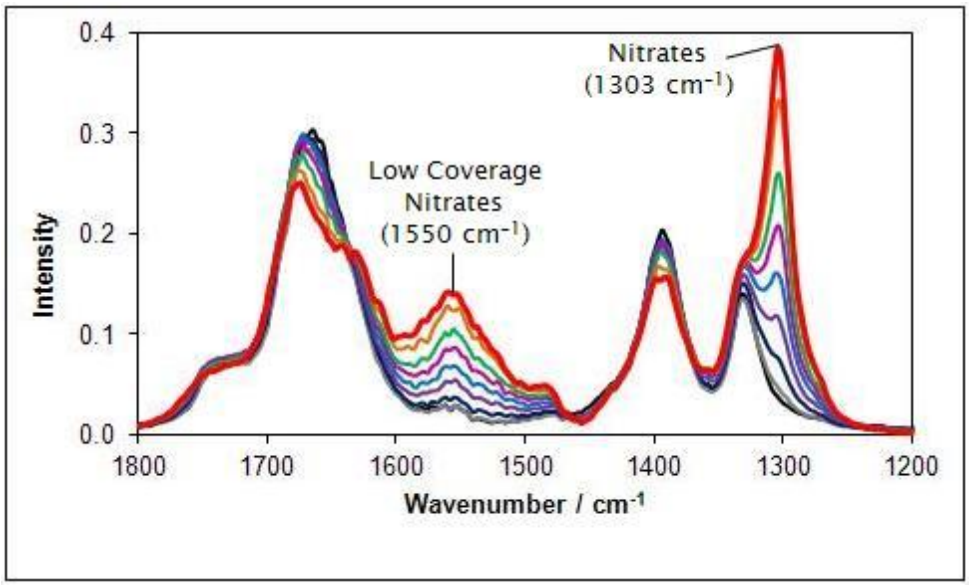

Figure 16: DRIFTS of 1 wt-% at 250℃ Pt/Al_2O_3 at 250℃ exposed to NO_2 + O_2 following exposure to C_3H_6 + O_2 for times 0, 10, 30, 60, 90, 120, 160, 230 and 320 min (black to red). Feed gas composition: 250 ppm NO_2, 5% O_2 and balance He.

The intensity of the band at 1665 cm^{-1}, due to C=O stretching, decreased slightly with time and shifted to 1677 cm^{-1} with two small shoulders at 1631 and 1641 cm^{-1} (carboxylate) becoming evident. Similarly, the bands at 1400 and 1332 cm^{-1}, assigned to formate species, also showed little change. The nitrate peak at 1303 cm^{-1}, previously attributed to monodentate nitrate species, appeared but its associated peak at 1585 cm^{-1} observed above did not, instead a band at 1554 cm^{-1} formed. This lower wavenumber band has been attributed to low coverage of either bidentate or monodentate nitrates [36]. Compared to NO_2 adsorption over, or interaction with, the clean Pt/Al_2O_3 surface, the rate of NO_2 adsorption over the C_3H_6 pre-adsorbed surface was significantly slower. This is evident by comparing the intensities between figures as well as noting that the low coverage 1554 cm^{-1} nitrate peak

remained after nearly 100 minutes of NO_x exposure compared to the same low coverage nitrate peak shifting to 1585 cm^{-1} within 20 minutes of NO_x exposure on the fresh catalyst. The peak intensities reached a saturation point after around 75 minutes, and the end result is that there were barely any nitrates formed when directly compared to the case when NO_x adsorbs on the fresh catalyst.

Recently, it was reported by Henry et al. [66] that adsorbed C_3H_6 can promote low temperature NO oxidation. They proposed that HC adsorbed on the surface can act as an oxygen sink to keep the Pt surface in a less oxidized state, which is beneficial for NO oxidation to NO_2. The DRIFTS results here indicate that less nitrates form on a surface with pre-adsorbed HC. Nitrates are also strong oxidants and since less nitrates formed, this could in turn lead to less extensive Pt surface oxidation. This might help explain the observed promotion of NO oxidation by stored HC noted in the previous research as well as the observed enhancement noted between 200 and 240℃ in Figure 10.

Finally, the clean catalyst was exposed to NO + C_3H_6 or NO_2 + C_3H_6 simultaneously in the presence of oxygen, to yield spectra shown in Figures 17a and 17b, respectively.

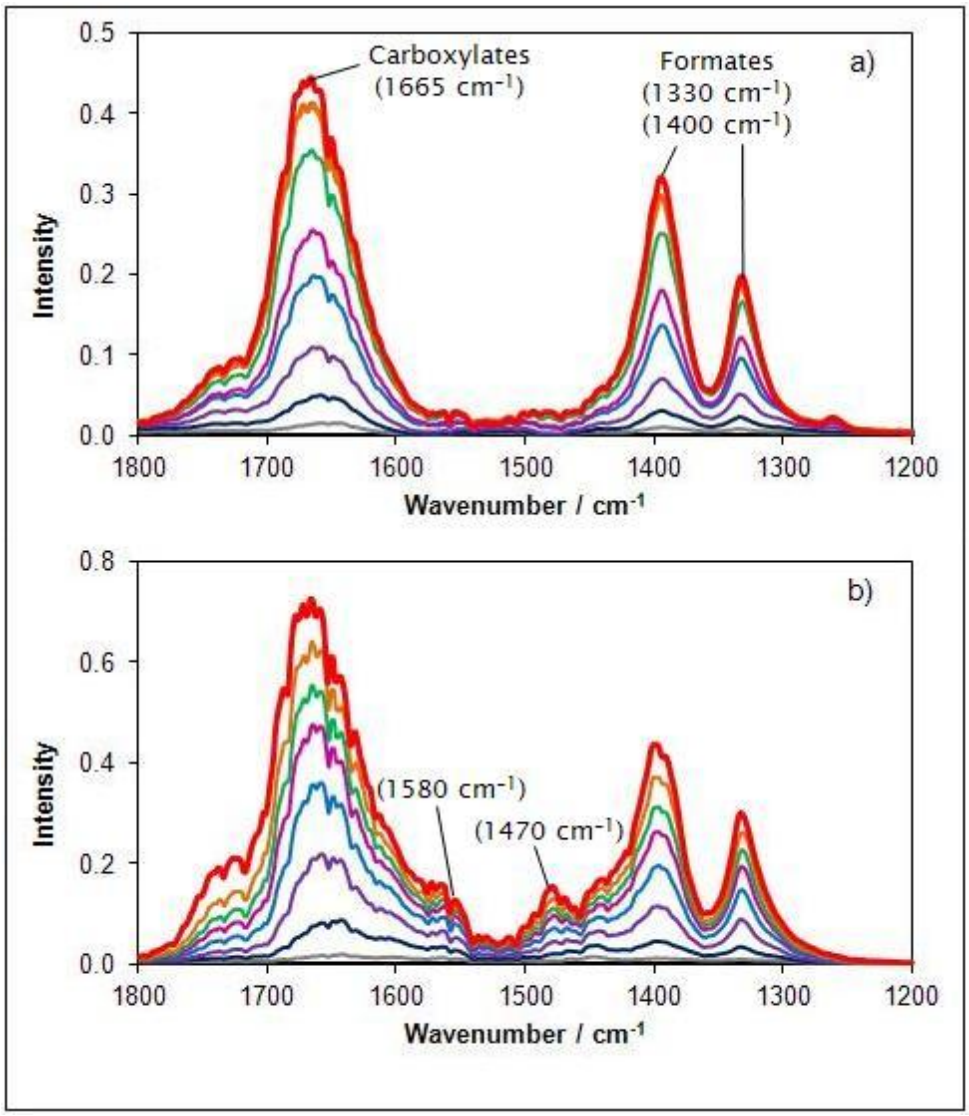

Figure 17: DRIFTS of 1 wt-% Pt/Al_2O_3 at 250°C exposed to: a) NO + C_3H_6 + O_2 for times 0, 10, 30, 60, 90, 110, 150, 200 and 290 min (black to red) and b) NO_2 + C_3H_6 + O_2 for times 0, 10, 30, 60, 90, 110, 150, 200 and 300 min (black to red). Feed gas composition: 250 ppm NO or NO_2, 200 ppm C_3H_6, 5% O_2 and balance He.

For NO and C_3H_6 co-addition, almost the same spectra were obtained as under C_3H_6-only conditions, with the bands at 1332, 1390–1400 and 1665 cm^{-1} attributed to the formation of

formate species. For NO_2 and C_3H_6, the spectra were essentially the same but with a minor peak at 1470 cm^{-1} also evident, which is relatively close to the 1463 cm^{-1} peak observed in Figure 13. Nitrate formation was not observed in these two sets of spectra. The reason is that the concentration of C_3H_6 (200 ppm) was relatively high, based on stoichiometry, which requires a high ratio of NO_x to C_3H_6 for the formation of nitrates and the reaction between nitrates and C_3H_6, compared to NO_x (250 ppm) in the feed. The experiment was therefore repeated with 1000 ppm NO and 100 ppm C_3H_6 and the resulting DRIFTS spectra are shown in Figure 18.

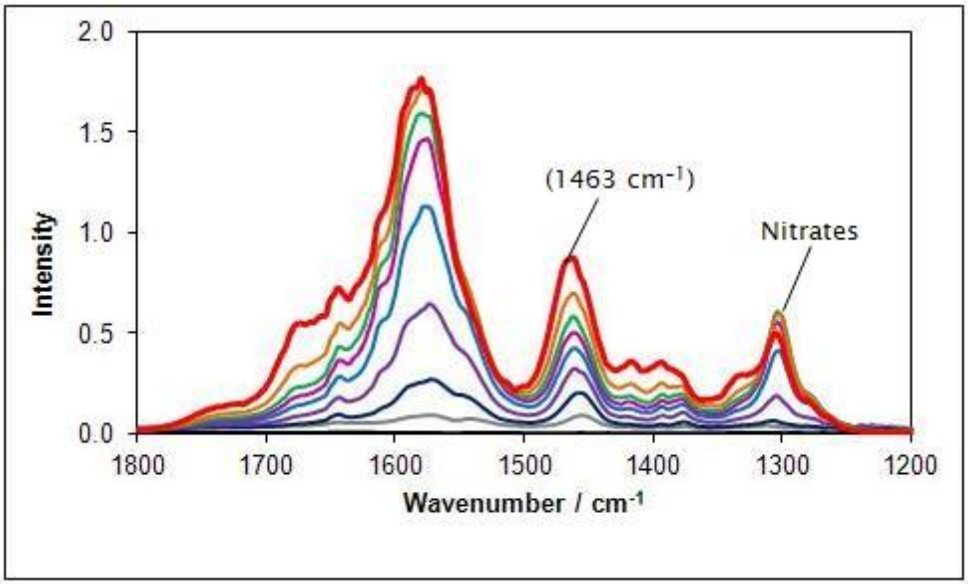

Figure 18: DRIFTS of 1 wt-% Pt/Al_2O_3 at 250℃ exposed to NO + C_3H_6 + O_2 for times 0, 5, 10, 15, 20, 25, 30, 40 and 60 min (black to red). Feed gas composition: 1000 ppm NO, 100 ppm C_3H_6, 5% O_2 and balance He.

These spectra are very similar to those with C_3H_6 exposure on the surface with pre-adsorbed nitrates. With the higher NO concentration in the feed, the nitrate bands at 1585 and 1303 cm^{-1} formed. As observed in the last few time points in the spectra shown in Figure 18, the 1303 cm^{-1} nitrate band decreased slightly, which indicates continued nitrate consumption, leading to the formation of the band at 1463 cm^{-1}. Such evidence of consumption was not observed for the nitrates in the 1585 cm^{-1} region because it overlaps with the carboxylate species bands formed in this same region. Overall, the higher concentration of NO in the feed allowed net nitrate formation on the surface. Nitrates can still react with C_3H_6, but are observed when NO_x is added in excess amounts relative to C_3H_6.

The band at 1463 cm^{-1} appeared when the catalyst was exposed first to NO_x and then to C_3H_6 after. This is directly related to the reaction between gas-phase C_3H_6 and stored nitrates. In the case of 250 ppm NO and 200 ppm C_3H_6 in the feed stream together, C_3H_6 was mainly oxidized mainly by O_2 and not by nitrates due to the excess amount of C_3H_6 relative to NO, and the 1463 cm^{-1} band was absent. In the case of NO_2 and C_3H_6 in the feed together, the formation of nitrates was relatively easier and faster. Thus, a portion of the C_3H_6 could be oxidized by nitrates in addition to O_2, which lead to the appearance of a small peak at 1470 cm^{-1} was observed, which is attributed to a low coverage nitrite peak. These results indicate that the surface nitrates may have been reduced to nitrite species by C_3H_6, with it most likely a linear nitrite, which has an IR band assignment at 1465 cm^{-1} [59,61]. However, a COO^- symmetric stretching vibration of adsorbed acetate ions [62–64] and acrylate species [61] has a similar band assignment so cannot be completely dismissed. The results of this study show surface nitrates do indeed react with C_3H_6, with the likely formation of linear nitrites.

Therefore, nitrates acting as the oxidant for C_3H_6 oxidation is a possible reaction pathway. The evidence, and possible relevance, strongly depends on the NO_x source (NO vs. NO_2) and inlet NO/C_3H_6 ratios. Using NO_2 instead of NO, or with a high NO_x/C_3H_6 ratio, some of the C_3H_6 can be oxidized via this nitrate as an oxidant route.

Chapter 5
Reaction Kinetics of C_3H_6 Oxidation for Various Reaction Pathways

5.1 Results and Discussion

In Chapter 4, it was discovered that surface NO_x species were shown to oxidize C_3H_6. However, which of the possible reactions, oxidation with O_2, NO_2 or nitrates, is more critical or relevant is not clear. Therefore, in this chapter, the kinetics of C_3H_6 oxidation via O_2, NO_2 and nitrates are compared. Since nitrates are readily formed by exposure of Pt/Al_2O_3 to NO_2, a different support had to be used to investigate C_3H_6 oxidation with only NO_2 as the oxidant (i.e. to avoid nitrates oxidizing the C_3H_6). Consequently, Pt/SiO_2 was used because SiO_2 is known to be relatively inert [33] and therefore should not adsorb any NO_x on its surface, allowing the isolation of the oxidizing nitrates or NO_2. NO_x adsorption over Pt/SiO_2 was evaluated with DRIFTS to confirm, and no surface NO_x species were formed as expected.

5.1.1 Determination of Pt Dispersion by H_2 Chemisorption

H_2 and CO chemisorption are commonly used to determine the precious metal dispersion and surface area in supported metal catalysts [67]. Under certain conditions, precious metals will chemisorb these gases stoichiometrically while the support will not. Typically the catalyst is heated and then reduced by H_2 prior to chemisorption. Past studies have shown that hydrogen adsorption on Pt is commonly used [67–70] so H_2 was chosen as the gas for chemisorption to determine the Pt dispersions. The pulse chemisorption method first reported by Gruber [69]

uses multiple pulses of adsorbate (H_2) of known volume, which are injected into a flow of inert gas and passed over the catalyst. H_2 adsorbs irreversibly onto Pt sites with each pulse until all the sites become saturated. Several fully eluted pulses are recorded at the end of the experiment and any partly adsorbed pulses are calibrated against the full pulses at the end to determine how much H_2 was chemisorbed on the metal. For H_2 chemisorption on Pt, a stoichiometric relation of two Pt sites for one molecule of H_2 is used [67, 69–70]. Each H_2 pulse is measured with a MS, with the data resulting in a "peak" of H_2. An example is shown in Figure 19.

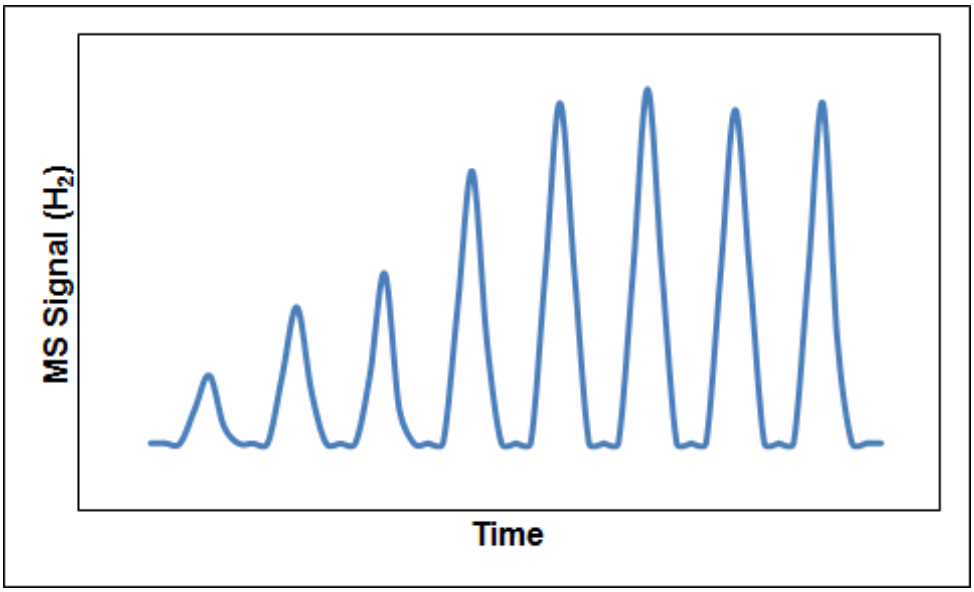

Figure 19: A sketch of H_2 chemisorption peaks collected by MS over time.

The area of each peak was calculated using the peak analyzer tool in Origin Pro 8. Pt dispersion (%) is calculated using equation (1).

$$\text{Pt Dispersion (\%)} = \left(\frac{\frac{A_S}{N_S} - \frac{A_A}{N_A}}{\frac{A_S}{N_S}} \right) \cdot \left(\frac{V_{H_2}}{V_{STP}} \right) \cdot \left(\frac{\upsilon_{Pt:H_2}}{m_{cat} \cdot \omega_{Pt}} \right) \cdot M_{Pt} \cdot 100\% \quad (1)$$

In this equation, A_S is the total area of the saturated peaks, N_S is the number of the saturated peaks, A_A is the total area of the adsorbed peaks, N_A is the number of adsorbed peaks, V_{H2} is the volume of H_2 pulsed into the reactor flow, V_{STP} is the standard volume of 22.4 L/mol, $\upsilon_{Pt:H2}$ is the 2:1 stoichiometric ratio of Pt sites to H_2, m_{cat} is the mass of the sample catalyst in the reactor, ω_{Pt} is the Pt loading (%) and M_{Pt} is the atomic weight of Pt. The dispersion values of the two catalyst samples are listed in Table II. Sample calculations are included in Appendix B.

Table II: Calculated Pt dispersion (%) of the sample catalysts.

Catalyst Type	Pt Dispersion (%)
Pt/SiO_2	1.6
Standard Pt/Al_2O_3	23.1
Aged Pt/Al_2O_3	1.3

The Pt/SiO_2 sample had a much lower Pt dispersion of 1.6% than the Pt/Al_2O_3 catalyst. Although not required for the kinetic analysis, it would be better if these dispersions were similar. H_2 chemisorption on the standard Pt/Al_2O_3 showed a higher dispersion, 23.1%. Therefore, it was thermally aged at 650℃ for two hours to sinter the particles and reduce the dispersion. After aging, the dispersion was reduced to 1.3%, which is relatively close to the Pt dispersion on Pt/SiO_2 sample.

The idea behind oxidizing C_3H_6 on two different supports was to determine the effect of nitrates on the oxidation reaction. As mentioned earlier, SiO_2 supports do not adsorb any NO_x on the surface, which was confirmed with the DRIFTS data obtained by Pieta [71] and displayed in Figure 19.

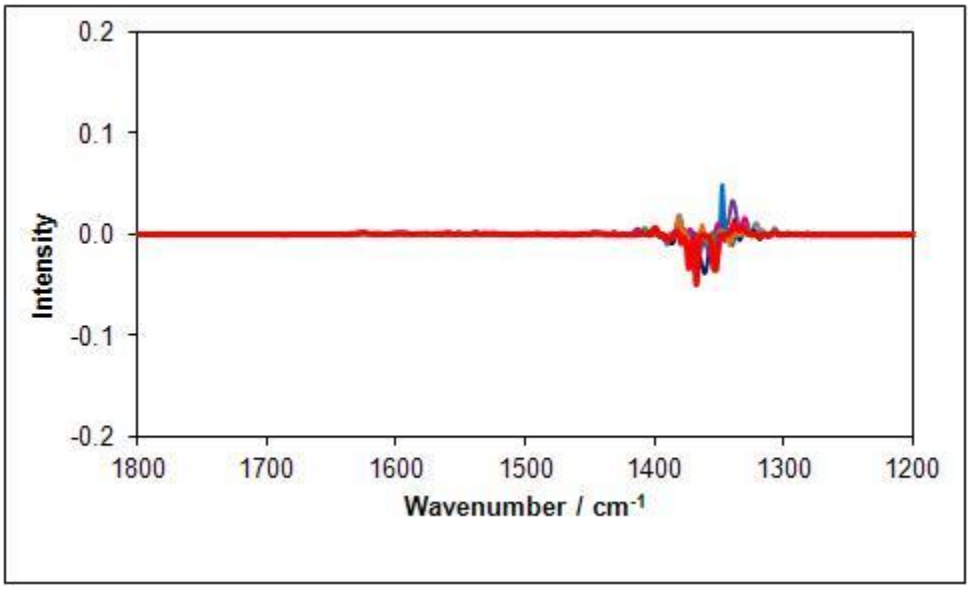

Figure 19: Sample IR spectra taken from flowing 200 ppm NO and 5% O_2 in He over Pt/SiO_2 catalyst [71].

At an inlet gas composition of 200 ppm NO and 5% O_2, only weak bands were observed, at about noise level. Also, following the NO_x adsorption experiments, the catalyst was heated and no NO_x desorption was observed.

5.1.2 Temperature Dependence of C_3H_6 Oxidation with O_2 and with NO_2

The temperature dependence of C_3H_6 oxidation with O_2 or NO_2 as the oxidant over the Pt/Al_2O_3 and Pt/SiO_2 catalysts was evaluated using TPO and a step ramp experiment. Concentration profiles as a function of temperature and/or time of C_3H_6 in the presence of O_2 and of NO_2 were obtained using CATLAB. The Arrhenius equation, $k = Ae^{-E/RT}$, where k is the specific reaction rate, A is the pre-exponential factor or frequency factor, E is the activation energy (J/mol), R is the gas constant (8.314 J $mol^{-1}K^{-1}$) and T is the absolute temperature (K), can be used to determine activation energies.. By taking the natural log of the equation, the equation becomes, ln k = ln A – E/R(1/T), which is used to derive the temperature dependence of a reaction [72]. The slope of the line (– E/R) of ln k versus 1/T can be used to calculate the apparent E. Morooka and Ozaki [73] showed that the reaction rate is proportional to the observed conversion (X); therefore, the slope calculated using the line of ln X vs 1/T is equivalent to the line of ln k vs 1/T. This was validated with the collected experimental data. The temperature range that resulted in low C_3H_6 conversion (< 15%) was used to calculate the apparent E for the C_3H_6 oxidation reaction, in order to apply the principles of a differential reactor [73–74]. By using the low conversion region, the reaction is kinetically limited, thereby avoiding mass transfer limitations. Also, this reduces the effect of the exotherm [17] so that the temperature used for the calculations reflects the actual temperature of the system. The Arrhenius plots for C_3H_6 oxidation with O_2 and with NO_2 are shown in Figure 20.

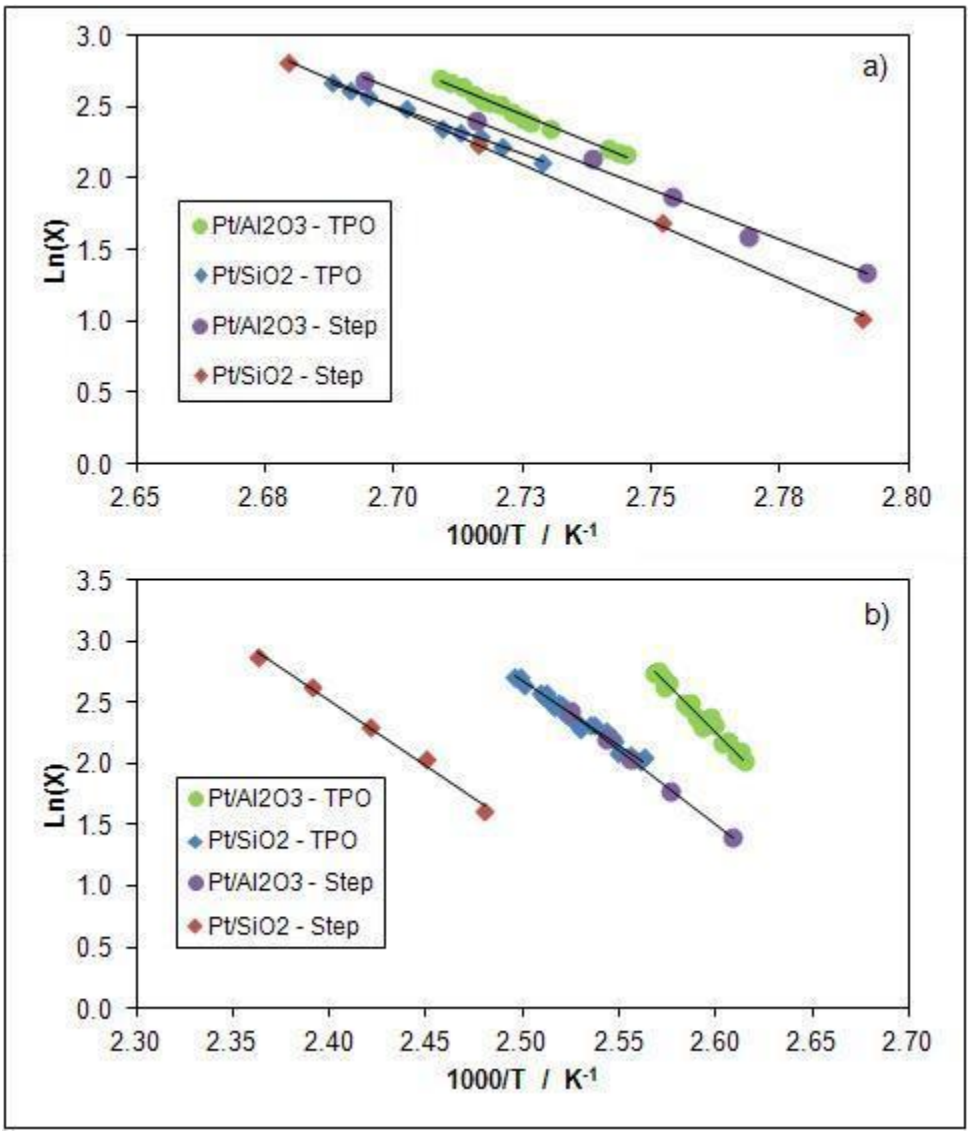

Figure 20: Arrhenius plot of C_3H_6 oxidation over Pt/Al_2O_3 and Pt/SiO_2 performed with two methods: TPO and step ramp with a) O_2 and b) with NO_2 as oxidant. Feed gases: 100 ppm C_3H_6, 6.5% O_2 or 1000 ppm NO_2, 200 ppm Ar and balance He.

A conversion range of 8 to 15% was used for the TPO experiments, while 4 to 15% was used for the step ramp experiments. Results revealed that these conversion ranges corresponded to temperature ranges for C_3H_6 oxidation with NO_2 for Pt/Al_2O_3 and Pt/SiO_2 to be from 105 to

120℃ and 120 to 150℃, respectively. With O_2, for both catalysts, the temperatures were in the 85 to 100℃ range. C_3H_6 oxidation with NO_2 began at a higher temperature (~92℃ for Pt/Al_2O_3 and ~90℃ for Pt/SiO_2) than with O_2 (~77℃ for both catalysts), which was not expected as the reported evidence suggests that NO_2 is a stronger oxidant than O_2. For example, soot oxidation occurs at lower temperatures with NO_2 than O_2 [75]. While NO_2 is a stronger oxidant, C_3H_6 or HC molecules may not interact the same way with NO_2 as soot does, NO_2 adsorbs directly to the soot surface, whereas in this process, the NO_2 adsorbs on the catalyst, on which HCs also adsorb.

The activation energy of the proposed oxidation reactions can be determined by first checking the linearity of the Arrhenius plot. The coefficients of determination (R^2) for all plots were at least 0.95 and the slope of each line was used to calculate the activation energy by multiplying the slope with R (8.314 J $mol^{-1}K^{-1}$). Each experiment was repeated at least once for reproducibility and the values were averaged. The errors of each slope (confidence interval) were also calculated at a 95% confidence level. Sample calculations are shown in Appendix B. Calculated activation energies with their 95% confidence interval are listed in Table III.

Table III: Calculated activation energy for C_3H_6 oxidation with O_2 and with NO_2.

Catalyst	Method	E (kJ/mol)	
		$C_3H_6 + O_2$	**$C_3H_6 + NO_2$**
Pt/Al_2O_3	TPO	143.9 ± 17.0	120.1 ± 8.7
Pt/SiO_2	TPO	112.6 ± 15.7	82.9 ± 3.1
Pt/Al_2O_3	Step Ramp	131.2 ± 13.5	110.9 ± 11.2
Pt/SiO_2	Step Ramp	137.8 ± 15.8	85.7 ± 6.8

The results show the E obtained from two methods: TPO and step ramp, are relatively close in all cases. Statistical evidence also confirmed this to be true with a t-test [76] at a 95% confidence level. This t-test performed for all oxidation reactions on both catalysts consistently showed that there were no significant differences between the TPO and step ramp method. If only the averages of the TPO and step ramp between C_3H_6 oxidation with O_2 and NO_2 over Pt/Al_2O_3 were considered, it does appear that with NO_2 as the oxidant, the activation energy is less than with O_2 (O_2 to NO_2 – TPO: 144 to 120 kJ/mol and Step Ramp: 131 to 111 kJ/mol). However, considering the errors, it is more difficult to distinguish between the calculated activation energies for Pt/Al_2O_3. On the other hand, for Pt/SiO_2, when comparing the activation energies of C_3H_6 oxidized by NO_2 and by O_2, a significant difference exists. The activation energy with NO_2 is significantly lower than with O_2. It is important to note that a significant difference is clearly observed when comparing the oxidants over Pt/SiO_2 and the only difference between Pt/Al_2O_3 and Pt/SiO_2 is that no surface NO_x species are formed over the SiO_2 support. Results show that less energy is required for C_3H_6 oxidation with NO_2 as the oxidant in the absence of nitrates; therefore, this suggests

that nitrates influence the kinetics of C_3H_6 oxidation with NO_x in the gas phase for a Pt/Al_2O_3 catalyst, which would be the case in real applications with actual exhaust gas.

5.1.3 Temperature Dependence of C_3H_6 Oxidation with Nitrates

To further investigate the effect of nitrates on C_3H_6 oxidation, the standard Pt/Al_2O_3 catalyst in powder form was first saturated with nitrates by exposing it to a stream of NO_2 and O_2 at 275℃ in the CATLAB. NO_2 was turned off and then cooled down and then the temperature was ramped in the presence of C_3H_6 to determine whether the nitrates can oxidize C_3H_6. C_3H_6 began to oxidize at about 190℃, which is much higher than with O_2 or NO_2; however, during a repeat of this experiment in the absence of C_3H_6, NO_x began to desorb at this temperature as well. The desorbed NO_x gave C_3H_6 a source of oxidant, which then resulted in the start of C_3H_6 oxidation. Without any oxidant in the gas phase, activation of C_3H_6 or HC molecule does not occur even with nitrates on the surface, prior to nitrate decomposition, and with nitrate decomposition the formed NO_2 can act as the oxidant. A similar effect was also observed by Irani et al. [12] where addition of HCs significantly decreased the NO_2 reduction temperature but to different extents depending on the HC that was correlated to the activation of HCs. It appears, based on these results, that in order for the nitrates to have an effect, C_3H_6 first has to be activated. Therefore, the experiment was repeated with C_3H_6 and O_2 instead of just C_3H_6.

In the presence of nitrates, C_3H_6 and O_2, C_3H_6 oxidation began at around 63℃, which was lower than the previous starting temperatures involving just O_2 or NO_2. Arrhenius plots from

8 to 15% conversion, which corresponded to a temperature range of 77 to 84℃, are displayed in Figure 21.

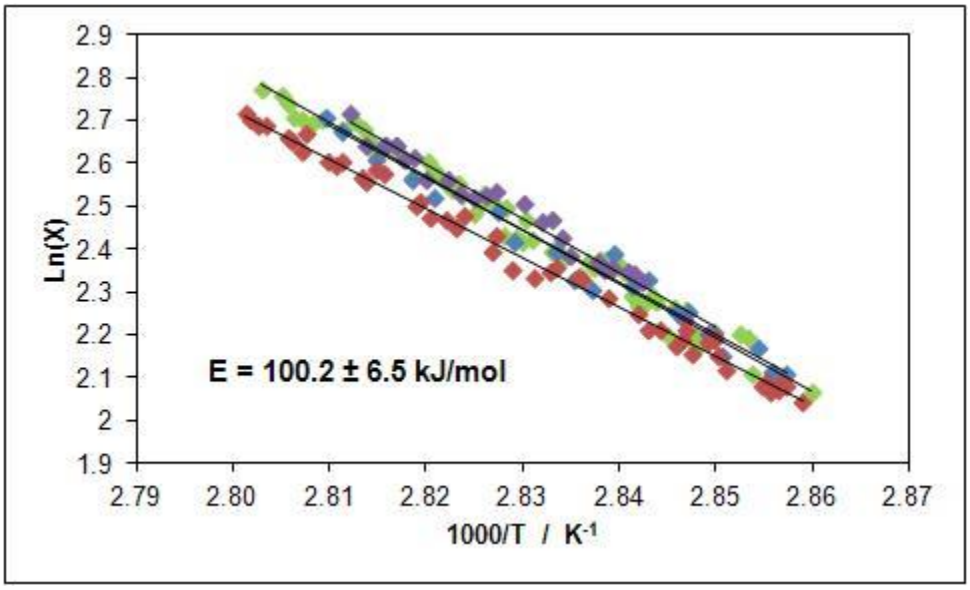

Figure 21: Arrhenius plots of C_3H_6 oxidation over Pt/Al_2O_3 in the presence of nitrates by TPO. Nitrates made with 500 ppm NO_2, 6.5% O_2, 200 ppm Ar and balance He (repeated 3 times). TPO gas mixture: 100 ppm C_3H_6, 6.5% O_2, 200 ppm Ar and balance He.

A consistent set of data was obtained from 4 separate experiments with all R^2 values greater than 0.97. Sample calculations are included in Appendix B. With O_2 and nitrates present, C_3H_6 oxidation starts earlier than with just O_2 or NO_2. This gives further indication that C_3H_6 must to be activated in order for the nitrates to have an effect. It was also confirmed that the nitrates were present even after C_3H_6 was completely oxidized as NO_x desorption was observed at higher temperatures. C_3H_6 oxidation reached completion at about 100℃ and NO_x began to desorb at about 190℃. The activation energy calculated from the Arrhenius

equation is approximately 100 kJ/mol. The activation energy of C_3H_6 oxidation with O_2 and nitrates is lower than that of the oxidation reactions with O_2 or NO_2. With the surface covered with nitrates, C_3H_6 oxidation occurs at a lower temperature and has a lower energy barrier as well. Just to confirm that NO_x desorption was not occurring on its own before C_3H_6 oxidation was complete, the temperature ramp portion of the experiment was repeated without C_3H_6 (only O_2). The temperature profiles of NO_x desorption with and without C_3H_6 are displayed in Figure 22.

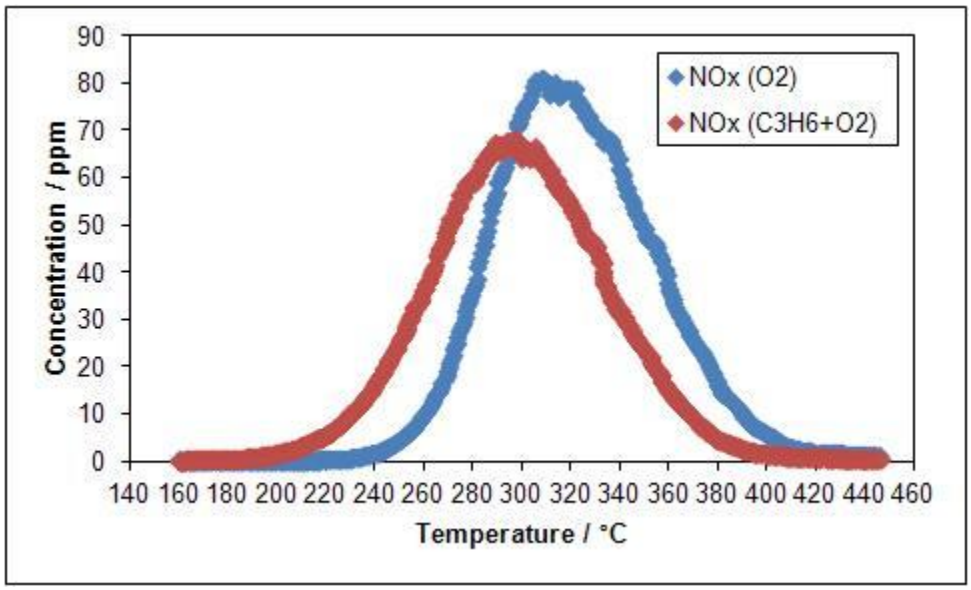

Figure 22: Temperature profiles of NO_x desorption with and without C_3H_6. Nitrates made with 500 ppm NO_2, 6.5% O_2, 200 ppm Ar and balance He. TPO gas mixture ◆: 100 ppm C_3H_6, 6.5% O_2, 200 ppm Ar and balance He; ◆: 6.5% O_2, 200 ppm Ar and balance He.

The results show that NO_x began to desorb at a higher temperature in the absence of C_3H_6. Previous research indicates that barium nitrates are more stable when O_2 is present, and this

apparently extrapolates to nitrates on the Al_2O_3 surface [77–78]. This was not the case when C_3H_6 was also present, NO_x began desorbing at the same temperature as it did during a TPD without any O_2 and C_3H_6. In the presence of C_3H_6, it is also apparent that less NO_x desorbed during the temperature ramp, based on Figure 22. To quantify the consumption of nitrates by C_3H_6 oxidation, the integrated areas of the NO_x desorption peaks are tabulated in Table IV.

Table IV: Total amount of NO_x desorbed during the temperature ramp with C_3H_6 and O_2 and with O_2.

Inlet gases	**Desorbed NO_x (ppm*s)**
100 ppm C_3H_6, 6.5% O_2, 200 ppm Ar, balance He	74068.3
6.5% O_2, 200 ppm Ar, balance He	81159.3

The amount of NO_x desorbed decreased by about 9% with C_3H_6 oxidation. This is consistent with the theory of nitrates being reduced by C_3H_6 as was noted in Chapter 4. When exposed to C_3H_6 and O_2 during the temperature ramp, less NO_x desorbed from the catalyst surface as some of it was consumed during C_3H_6 oxidation.

The results of this study showed that nitrates do indeed play a role in C_3H_6 oxidation, causing the reaction to occur at lower temperatures, and with a lower activation energy based on the obtained reaction kinetics data. It also added further evidence that HCs must be activated in order for NO_x to have any effect on HC oxidation.

Chapter 6
Conclusions

Diesel oxidation catalysts are a critical component of diesel exhaust aftertreatment systems. DOCs readily oxidize CO and HC species but also oxidize NO to NO_2. Oxidizing NO to NO_2 does not reduce the total NO_x level; however, higher NO_2 concentrations improve NO_x storage on downstream NO_x traps, improve the low temperature efficiency of SCR catalysts, and lower the soot oxidation temperatures on particulate filters [17]. DOCs commonly consist of precious metals, such as Pt, for their oxidation ability and a high surface area support, such as Al_2O_3 to disperse the metal. A pilot reactor, CATLAB and DRIFTS were used to investigate the interaction between surface NO_x species and HCs.

TPO experiments on a Pt/Al_2O_3 monolith catalyst in a pilot reactor system showed definite low temperature inhibition of NO oxidation by C_3H_6 and vice versa. C_3H_6 oxidation is inhibited by competitive active site adsorption while NO oxidation inhibition is explained by active site adsorption inhibition as well as the product NO_2 being consumed as an oxidant for C_3H_6 oxidation. On CATLAB, NO_x TPD experiments were performed with a powder Pt/Al_2O_3 catalyst. When the adsorbed NO_x was exposed to C_3H_6 prior to the TPD, around 50% of the adsorbed NO_x was consumed which confirmed that C_3H_6 can react with the surface NO_x species. Using DRIFTS, it was determined that exposing Pt/Al_2O_3 to NO_x led to formation of surface nitrates. When the surface nitrates were exposed to C_3H_6 and O_2, the nitrates were consumed and a new species formed, which could be identified as either linear nitrites from the nitrates being reduced by subsequent C_3H_6 exposure or HC intermediates

from C_3H_6 oxidation. Additional experiments with different sequences of gas exposure show that the new species formed on the surface were most likely nitrites. The results indicate that surface nitrates can indeed act as an oxidant for C_3H_6 oxidation and in order for clear evidence of this reaction to occur, a high inlet NO_x to C_3H_6 ratio is required, or it was also readily evident with NO_2 as the NO_x source.

With evidence suggesting that surface NO_x species can oxidize C_3H_6, it added to the possible sources of oxidant for C_3H_6 oxidation, O_2 and NO_2. Reaction kinetics studies were done for the three possible oxidants in C_3H_6 oxidation over Pt/Al_2O_3 and Pt/SiO_2 in CATLAB. Since nitrates are readily formed on Pt/Al_2O_3 catalysts with NO_2, a Pt/SiO_2 catalyst, which is known to be inert toward nitrate formation, was used to isolate the reaction between C_3H_6 and NO_2. Pt dispersions of the Pt/Al_2O_3 and Pt/SiO_2 samples, determined by H_2 chemisorption, were 1.3 and 1.6%, respectively.

C_3H_6 oxidation with O_2 and NO_2 were performed with two different methods: TPO and step ramp on CATLAB for both Pt/Al_2O_3 and Pt/SiO_2. Statistical analysis showed there was no significant difference between the activation energies calculated from the two methods. C_3H_6 oxidation began earlier with O_2 than with NO_2 but the activation energy was lower for the reaction between C_3H_6 and NO_2 for Pt/SiO_2. These results suggest that HCs need to be activated first for NO_2 to be favored in HC oxidation. On Pt/Al_2O_3, the activation energies between C_3H_6 oxidation with O_2 and NO_2 were not significantly different, which suggests that nitrates have an effect on the kinetics of C_3H_6 oxidation. When the experiment was conducted with nitrates and C_3H_6 present, the reaction did not occur until NO_x began to

desorb from the catalyst. The stored NO_x desorbed at higher temperatures as it became thermally unstable and began to react with C_3H_6, which gave further evidence that C_3H_6 needs to be activated in order for NO_x to have any effect, whether it be surface nitrates or gas phase NO_2. Therefore, C_3H_6 and O_2 were exposed to the nitrates during the temperature ramp and C_3H_6 oxidation began earlier than with O_2 by itself. It not only proved that nitrates affect C_3H_6 oxidation once it becomes activated, but also results in a lower activation energy than C_3H_6 oxidation with O_2 (without nitrates). Also, nitrate consumption was observed during C_3H_6 oxidation as less NO_x desorbed from the catalyst than when the temperature was ramped in just O_2 (no C_3H_6 exposure), which was consistent with the DRIFTS results showing nitrate consumption during C_3H_6 oxidation.

Chapter 7
Recommendations

Based on the results obtained, further experiments can be envisioned to validate the findings at different scales, as well as to more accurately determine some of the values calculated. These are:

- Add more thermocouples inside the monolith sample to more accurately determine the temperature distribution within the catalyst to observe the exotherm effect of HC oxidation.
- Repeat experiments with Pd catalysts or Pt-Pd catalysts to compare the results to the results from this thesis, which only evaluated a Pt/Al_2O_3 catalyst - there is a lack of literature data available for Pd catalysts
- Formulate a Pt/SiO_2 monolith catalyst to perform the experiments from Chapter 5 on a pilot reactor to compare the data obtained from CATLAB.
- Install a USB – Ethernet adaptor to connect the OMNISTAR to the computer controlling CATLAB reactor. It can help as both devices could be remotely controlled away from the laboratory. The current setup has the MS connected to a different computer as all the Ethernet ports are used up on the CATLAB computer.
- Kinetics study done in Chapter 5 could be repeated involving other gases such as CO and/or NO to simulate actual exhaust.
- The outlet of the DRIFTS should be connected to the MS to measure outlet gases while simultaneously observing what is occurring on the catalyst surface.

References

[1] K. Skalska, J.S. Miller, S. Ledakowicz (2010) *Sci Total Environ* 408:3976.

[2] DieselNet "Gaseous Emissions" 2010. Retrieved Mar 2, 2012: http://www.dieselnet.com/tech/emi_gas.php

[3] W.A. Majewski, M.K. Khair. *Diesel Emissions and Their Control,* 2006. SAE International: Warrendale, PA.

[4] DieselNet "Diesel Emission Formation" 2008. Retrieved Mar 2, 2012: http://www.dieselnet.com/tech/diesel_emiform.php

[5] Environment Canada "Cars, Trucks, Vans and Sport Utility Vehicles" 2012. Retrieved Mar 4, 2012: http://www.ec.gc.ca/Air/default.asp?lang=En&n=EC8E75D0

[6] U.S. Department of Transportation "Transportation and Greenhouse Gas Emissions" 2006. Retrieved Mar 4, 2012: http://climate.dot.gov/about/transportations-role/overview.html

[7] DieselNet "Diesel Emission Control" 2007. Retrieved Mar 4, 2012: http://www.dieselnet.com/tech/engine_control.php

[8] DieselNet "Emission Standards" 2010. Retrieved Feb 14, 2012: http://www.dieselnet.com/standards

[9] R.M. Heck, R.J. Farrauto, *Catalytic Air Pollution Control, Commercial Technology,* 2nd Edition. 2002. John Wiley and Sons, New York, NY.

[10] Autos.ca “Motoring Memories: Diesel Cars in North America” 2007. Retrieved April 21, 2012: http://www.autos.ca/motoring-memories/motoring-memories-diesel-cars-in-north-america

[11] DieselNet “Diesel Catalysts” 2004. Retrieved Mar 15, 2012: http://www.dieselnet.com/tech/cat_diesel.php

[12] K. Irani, W.S. Epling, R. Blint. (2009) *Appl Catal B* 92:422.

[13] L. Castoldi, R. Matarrese, L. Lietti, P. Forzatti (2006) *Appl Catal B* 64: 25.

[14] F. Haass, H. Fuess (2005) *Adv Eng Mater 7:*899.

[15] L. Castoldi, R. Matarrese, L. Lietti, P. Forzatti (2006) *Appl Catal B* 64: 25.

[16] DieselNet “Catalytic Converters” 2004. Retrieved Mar 15, 2012: http://dieselnet.com/tech/cat_conv.php

[17] A. Russell, W.S. Epling (2011) *Catal Rev Sci Eng* 53:337.

[18] M.V. Twigg (2011) *Catal Today* 163:33.

[19] T. Kolli, M. Huuhtanen, T. Kanerva, M. Vippola, K. Kallinen, T. Kinnunen, T. Lepisto, J. Lahtinen, R.L. Keiski (2011) *Top Catal* 54:1185.

[20] T. Kanerva, V. Kroger, K. Rahkamaa-Tolonen, M. Vippola, T. Lepisto, R.L. Keiski (2007) *Top Catal* 45:137.

[21] M. Kaneeda, H. Iizuka, T. Hiratsuka, N. Shinotsuka, M. Arai (2009) *Appl Catal B* 90:564.

[22] D.L. Mowery, R.L. McCormick (2001) *Appl Catal B* 34:287.

[23] R. Burch, P.J. Millington (1996) *Catal Today* 29:37.

[24] Y.D. Kim, S.J. Jeong, W.S. Kim (2009) *Chem Eng Sci* 64:1373.

[25] M.A. Suad, J. Soares, W.S. Epling (2012) *Ind Eng Chem Res* 51:6672.

[26] S. Tronci, R. Baratti, A. Gavriilidis (1999) *Chem Eng Commun* 173:53.

[27] A. Russell, W.S. Epling, H. Hess, H.Y. Chen, N.W. Currier, A. Yezerets (2010) *Ind Eng Chem Prod Res Dev* 48:10311.

[28] C.K. Lambert, Y. Cheng, D. Dobson, J. Hangas, M. Jagner, H. Jen, J. Warner (2009) *SAE Technical Paper Series* 2009-01-2711.

[29] A.K. Neyestanaki, F. Klingstedt, T. Salmi, D.Y. Murzin (2004) *Fuel* 83:395.

[30] U. Lassi "Deactivation Correlations of Pd/Rh Three-way Catalysts Designed for EuroIV Emission Limits: Effect of Ageing Atmosphere, Temperature and Time" 2003. Retrieved Jan 12, 2012: http://herkules.oulu.fi/isbn9514269543

[31] W.S. Epling, L.E. Campbell, A. Yezerets, N.W. Currier, J.E. Parks II, (2004) *Catal Rev Sci Eng* 46:163.

[32] L. Olsson, B. Westerberg, H. Persson, E. Fridell, M. Skoglundh, B. Andersson (1999) *J Phys Chem B* 103:10433.

[33] E. Xue, K. Seshan, J.R.H. Ross (1999) *Appl Catal B* 11:65.

[34] L. Olsson, H. Persson, E. Fridell, M. Skoglundh, B. Andersson (2001) *J Phys Chem B* 105:6895

[35] S.S. Mulla, N. Chen, L. Cumaranatunge, G.E. Blau, D.Y. Zemlyanov, W.N. Delgass, W.S. Epling, F.H. Ribeiro (2006) *J Catal* 241:389.

[36] B. Westerberg, E. Fridell (2001) *J Mol Catal A: Chem* 165:249.

[37] P. Denton, A. Giroir-Fendler, H. Prailaud, M. Primet (2000) *J Catal* 189:410.

[38] L. Olsson, E. Fridell (2002) *J Catal* 210:340.

[39] D.H. Parker, M.E. Bartram, B.E. Koel (1989) *Surface Science* 217:489

[40] T. Tanabe, Y. Nagai, K. Dohmae, N. Takagi, N. Takahashi, S. Matsumoto, H. Shinjoh (2011) *Appl Catal B* 105:41.

[41] S.E. Voltz, C.R. Morgan, D. Liederman, S.M. Jacob (1973) *Ind Eng Chem Prod Res Dev* 12:294.

[42] F. Mittendorfer, C. Thomazeau, P. Raybaud, H. Toulhoat (2003) *J Phys Chem B* 107:12287.

[43] G. Mabilon, D. Durand, P. Courty (1995) *Stud Surf Sci Catal* 96:775.

[44] S. Benard, L. Retailleau, F. Gaillard, P. Vernoux, A. Giroir-Fendler (2005) *Appl Catal B* 55:11.

[45] P. Denton, A. Giroir-Fendler, H. Praliaud, M. Primet (2001) *Top Catal* 16-17:377.

[46] P. Briot, A. Auroux, D. Jones, M. Primet (1990) *Appl Catal* 59:141.

[47] B. Grbic, N. Radic, A. Terlecki-Baricevic (2004) *Appl Catal B* 50:161.

[48] M. AL-Harbi, R. Hayes, M. Votsmeier, W.S. Epling, (2011) *Can J Chem Eng* doi: 10.1002/cjce.20659

[49] Y. Ji, T.J. Toops, J.A. Pihl, M. Crocker (2009) *Appl Catal B* 91: 329.

[50] C. Sedlmair, K. Seshan, A. Jentys, J.A. Lercher (2003) *J Catal* 214: 308.

[51] T.J. Toops, D.B. Smith, W.P. Partridge (2006) *Catal Today* 114: 112.

[52] I.S. Pieta, M. Garcia-Dieguez, C. Herrera, M.A. Larrubia, L.J. Alemany (2010) *J Catal* 270:256.

[53] M. Haneda, M. Sasaki, H. Hamada, M. Ozawa (2011) *Catal Lett* 141: 1262.

[54] J.A. Anderson, C.H. Rochester (1989) *J Chem Soc Faraday Trans* 85:1117.

[55] G. Busca, J. Lamotte, J.C. Lavalley, V. Lorenzelli (1987) *J Am Chem Soc* 109: 5197.

[56] T. Chafik, S. Kameoka, Y. Ukisu, T. Miyadera (1998) *J Mol Catal A: Chem* 136: 203.

[57] W.S. Epling, C.H.F. Peden, J. Szanyi (2008) *J Phys Chem C* 112: 10952.

[58] V. Ermini, E. Finocchio, S. Sechi, G. Busca, S. Rossini (2000) *Appl Catal A* 190: 157.

[59] V. Matsouka, M. Konsolakis, R.M. Lambert, I.V. Yentekakis (2008) *App Catal B* 84:715.

[60] F.C. Meunier, J.P. Breen, V. Zuzaniuk, M. Olsson, J.R.H. Ross (1999) *J Catal* 187: 493.

[61] F.C. Meunier, V. Zuzaniuk, J.P. Breen, M. Olsson, J.R.H. Ross (2000) *Catal Today* 59: 287.

[62] D.K. Captain, M.D. Amiridis (1999) *J Catal* 184: 377.

[63] P.A. Kumar, M.P. Reddy, L.K. Ju, B. Hyun-Sook, H.H. Phil (2008) *J Mol Catal A: Chem* 291: 66.

[64] K. Shimizu, H. Kawabata, A. Satsuma, T. Hattori (1999) *J Phys Chem B* 103:5240.

[65] N. Sivasankar, H. Frei (2011) *J Phys Chem C* 115: 7545.

[66] C. Henry, N. Currier, N. Ottinger, A. Yezerets, M. Castagnola, H.Y. Chen, H. Hess (2011) *SAE Technical Paper Series* 2011-01-1137.

[67] J. Freel (1971) *J Catal* 25: 139.

[68] G.R. Wilson, W.K. Hall (1969) *J Catal* 17:190.

[69] H.L. Gruber (1962) *J Phys Chem* 66:48.

[70] J. Dawody, L. Eurenius, H. Abdulhamid, M. Skoglundh, E. Olsson, E. Fridell (2005) *Appl Catal A* 296:157.

[71] I.S. Pieta "CeO_2, Pt/CeO_2, SiO_2 and Pt/SiO_2 DRIFTS Results and Discussion" unpublished.

[72] H.S. Fogler, *Elements of Chemical Reaction Engineering*, 4th Edition. 2006. Pearson Education, Inc., Upper Saddle River, NJ.

[73] Y. Morooka, A. Ozaki (1966) *J Catal* 5:116.

[74] P. Gelin, M. Primet (2002) *Appl Catal B* 39:1.

[75] M. Shrivastava, A. Nguyen, Z. Zheng, H. Wu, H.S. Jung (2010) *Environ Sci Technol* 44:4796.

[76] D.C. Montgomery, *Design and Analysis of Experiments*, 6th Edition. 2005. John Wiley and Sons, New York, NY.

[77] J.A. Anderson, A.J. Paterson, M. Fernandez-Garcia (2000) *Stud Surf Sci Catal* 130:1331.

[78] K. Eguchi, T. Hayashi (1998) *Catal Today* 45:109.

[79] W.S. Kijlstra, D.S. Brands, H.I. Smit, E.K. Poels, A. Bliek (1997) *J Catal* 171:219.

[80] J.H. Lee, H.H Kung (1998) *Catal Lett* 51:1.

Appendix A
Addendum to Chapter 4

Additional experiments were performed to support the discussion presented in Chapter 4 "NO Oxidation Inhibition by HCs over a DOC – Reaction Between Surface Nitrates and HCs". In Chapter 4, a Pt/Al_2O_3 sample was evaluated at one temperature, 250℃. In this Appendix, the reaction over Al_2O_3 and over Pt/Al_2O_3 at other temperatures was investigated. Also, the reaction was performed in a pilot reactor system as well.

A.1 Experimental Methods

Using the same 1 wt-% $Pt/\gamma\text{-}Al_2O_3$ powder sample, the temperature effect on the reaction between surface nitrates and C_3H_6 was investigated using DRIFTS. The same equipment setup and pretreatment method as previously described in Chapter 3.2.1 were used. To characterize the interaction between gas-phase C_3H_6 and surface nitrates, 600 ppm NO_2, 5% O_2 and balance He were first introduced at 250℃ in order to form surface nitrites/nitrates. Once the nitrate peaks reached a saturation point, NO_2 was turned off and then the temperature was lowered to 200℃ in one experiment and 150℃ in another experiment in just 5% O_2 in He. The nitrates on the Pt/Al_2O_3 catalyst are thermally stable when formed at temperatures below 300℃ [31,36]. 200 ppm C_3H_6, 5% O_2 and balance He were introduced to investigate the reaction between C_3H_6 and nitrates at different temperatures. The same experiment was performed at 250℃ for pure Al_2O_3 sample as well.

For the pilot reactor study, a monolith sample of 1 in diameter and 2 in length with an Al_2O_3 loading of 1.59 g/in^3 and a Pt loading of 20 g/ft^3 was used. TPD experiments were performed to quantify the reaction between stored NO_x species and HC. 1000 ppm NO_2, 6.5% O_2 and balance N_2 were introduced at 270℃ for 1.5 hours, then NO_2 and O_2 were turned off and the temperature was ramped to 515℃ at 10℃/min. This experiment was then repeated twice more, with 10 second pulses of 20 ppm C_3H_6 for 2 minutes (6 total pulses) and for 5 minutes (15 total pulses) prior to the temperature ramp. The pulses were performed with a 4-way actuated switching valve to alternate the gas manifolds between 100% N_2 and 20 ppm C_3H_6 in N_2.

A.2 Results and Discussion

A.2.1 DRIFTS

Nitrates were formed at 250℃ by exposing Pt/Al_2O_3 to 1000 ppm and 6.5% O_2 in He on Pt/Al_2O_3 and after reaching a saturation point (prior to C_3H_6 addition), the temperature was lowered to 200 and 150℃, in two separate experiments, in O_2 and He, and the nitrates remained stable as expected [36,79]. 200 ppm C_3H_6, 5% O_2 and balance He were introduced and the resulting IR spectra are shown in Figure 23.

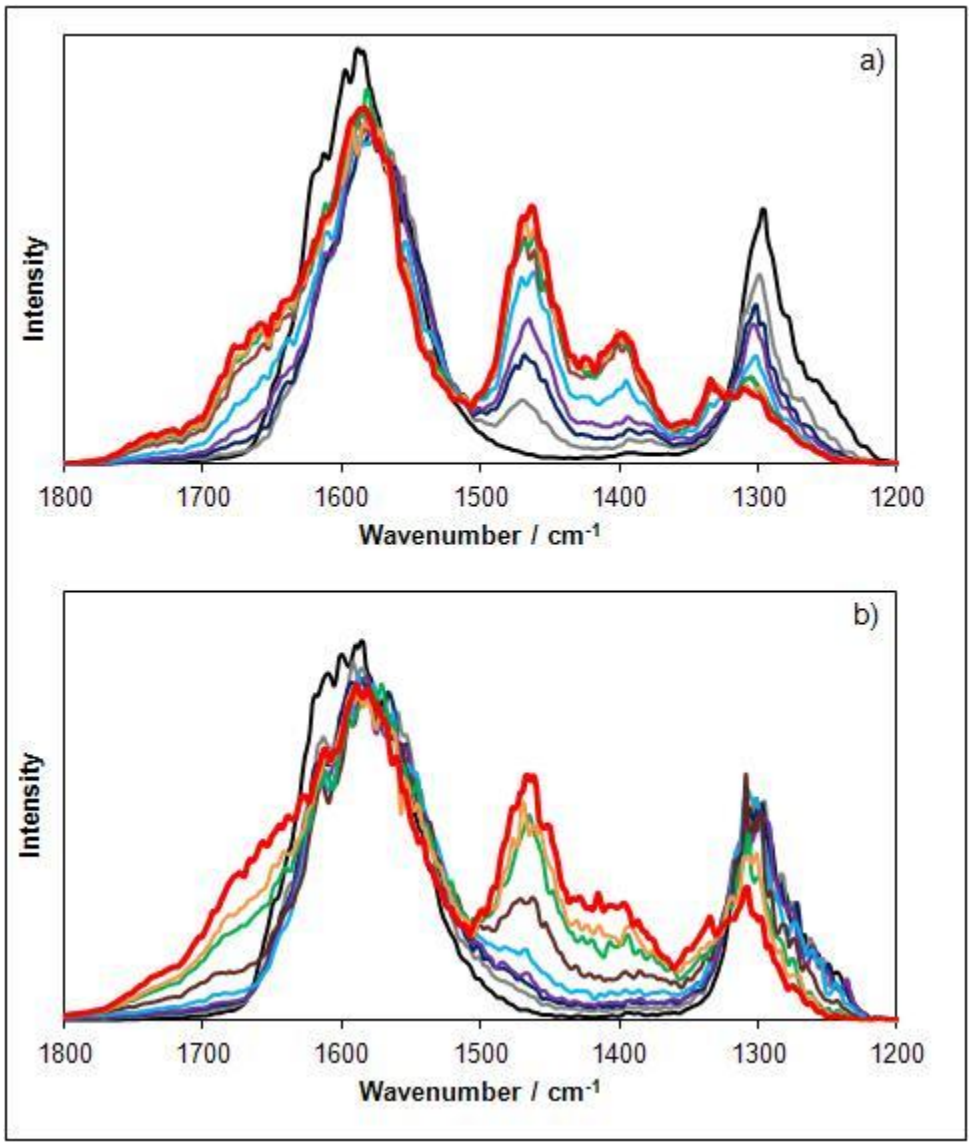

Figure 23: DRIFTS of 1 wt-% Pt/Al_2O_3 exposed to C_3H_6 + O_2 following exposure to NO_2 and O_2 for times 0, 5, 10, 15, 30 ,60, 90, 100 and 130 min (black to red) at (a) 200℃ and (b) 150℃. Feed gas composition: 200 ppm C_3H_6, 5% O_2 and balance He.

The same features and trends were observed as those at 250℃ with the only difference being at 250℃ (Chapter 4, Figure 13), the nitrate peak at 1303 cm^{-1} was almost completely reduced, over 80% of its original intensity, but at lower temperatures (Figure 23), the nitrate

peak was still visible at the end of the experiment as it had decreased by around 70% and 30% at 200℃ and 150℃, respectively. The same reactions were occurring but simply not as fast at lower temperature.

The reactivity between nitrates and C_3H_6 on an Al_2O_3 sample was also studied. While nitrates form on the Al_2O_3 surface when exposed to NO and O_2, this does not occur without Pt. Only a very small amount of nitrites may form and NO_x storage is also known to be difficult on Al_2O_3 alone; however, exposure to NO_2 and O_2 does lead to the formation of nitrates on Al_2O_3 (no Pt) [36]. The DRIFTS results obtained after exposing the Al_2O_3 sample to NO_2 and O_2 for 110 minutes are displayed in Figure 24.

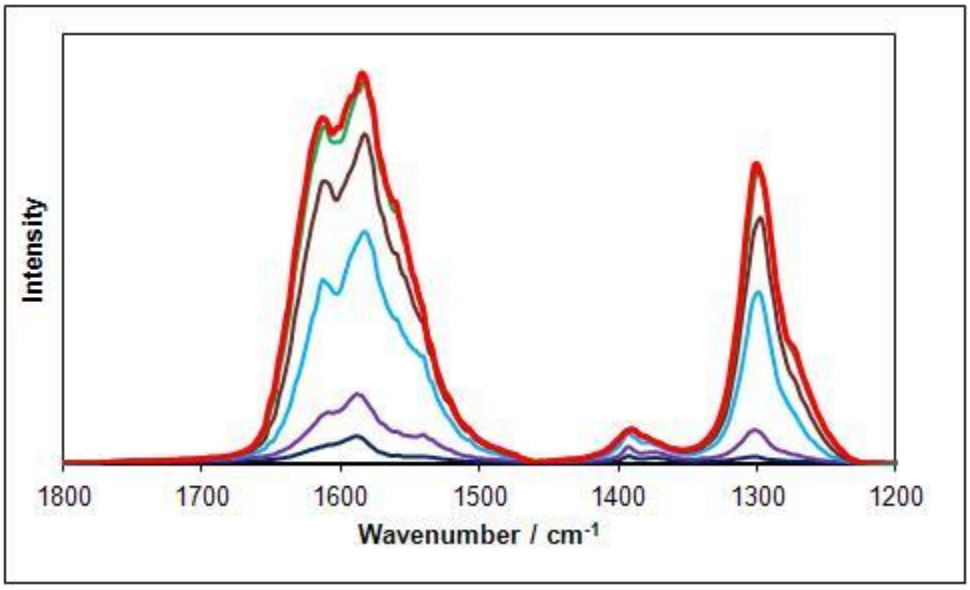

Figure 24: DRIFTS of γ-Al_2O_3 at 250℃ exposed to NO_2 + O_2 for times 0, 5, 15, 30, 60, 90 and 110 min (black to red). Feed gas composition: 600 ppm NO, 5% O_2 and balance He.

The same nitrate peaks observed on the Pt/Al_2O_3 sample were observed here at 1303 and 1585 cm^{-1}. The nitrate peak in the 1500 – 1700 cm^{-1} region was more defined, with peaks at 1585 and 1610 cm^{-1}, representing monodentate and bidentate nitrates, respectively [36,79]. Also, a distinct peak at 1393 cm^{-1}, which was not present in data obtained from the Pt/Al_2O_3 sample, was identified as bulk nitrate on Al_2O_3 ($Al^+NO_3^-$) [36]. After the nitrates were formed, the flow of NO_2 was turned off and C_3H_6 was introduced; results are displayed in Figure 25.

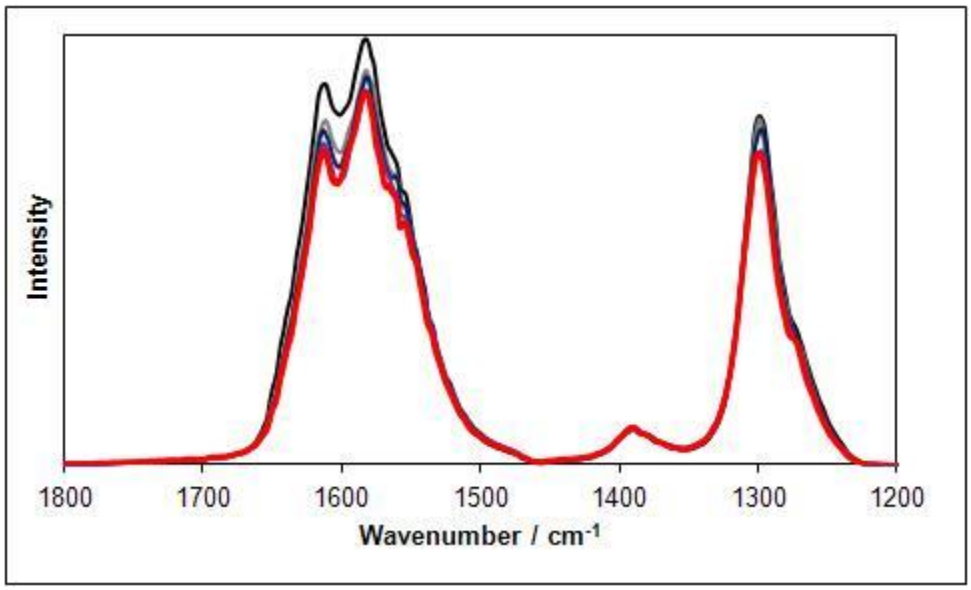

Figure 25: DRIFTS of γ-Al_2O_3 at 250℃ exposed to C_3H_6 + O_2 following exposure to NO_2 and O_2 for times 0, 10, 20, 35 and 70 min (black to red). Feed gas composition: 200 ppm C_3H_6, 5% O_2 and balance He.

After 70 minutes, the nitrate peak at 1303 cm^{-1} slightly decreased (around 10%); however, no significant reaction occurred, as was the case with the Pt/Al_2O_3 sample where the nitrates

were reduced to nitrites. The reaction was either extremely slow, but most likely does not occur without Pt present.

A.2.2 Pilot Reactor

To further validate the theory of nitrates being reduced by C_3H_6, TPD experiments on the monolith-supported catalyst in the pilot reactor were performed. First, nitrates were formed at 275℃, similar to the DRIFTS experiment. After the flow of NO_2 and O_2 were turned off, the temperature was ramped to 515℃ with only N_2 flowing for TPD. The experiment was repeated including a C_3H_6 pulse step prior to the temperature ramp (6 and 15 pulses of 20 ppm C_3H_6). TPD results are shown in Figure 26.

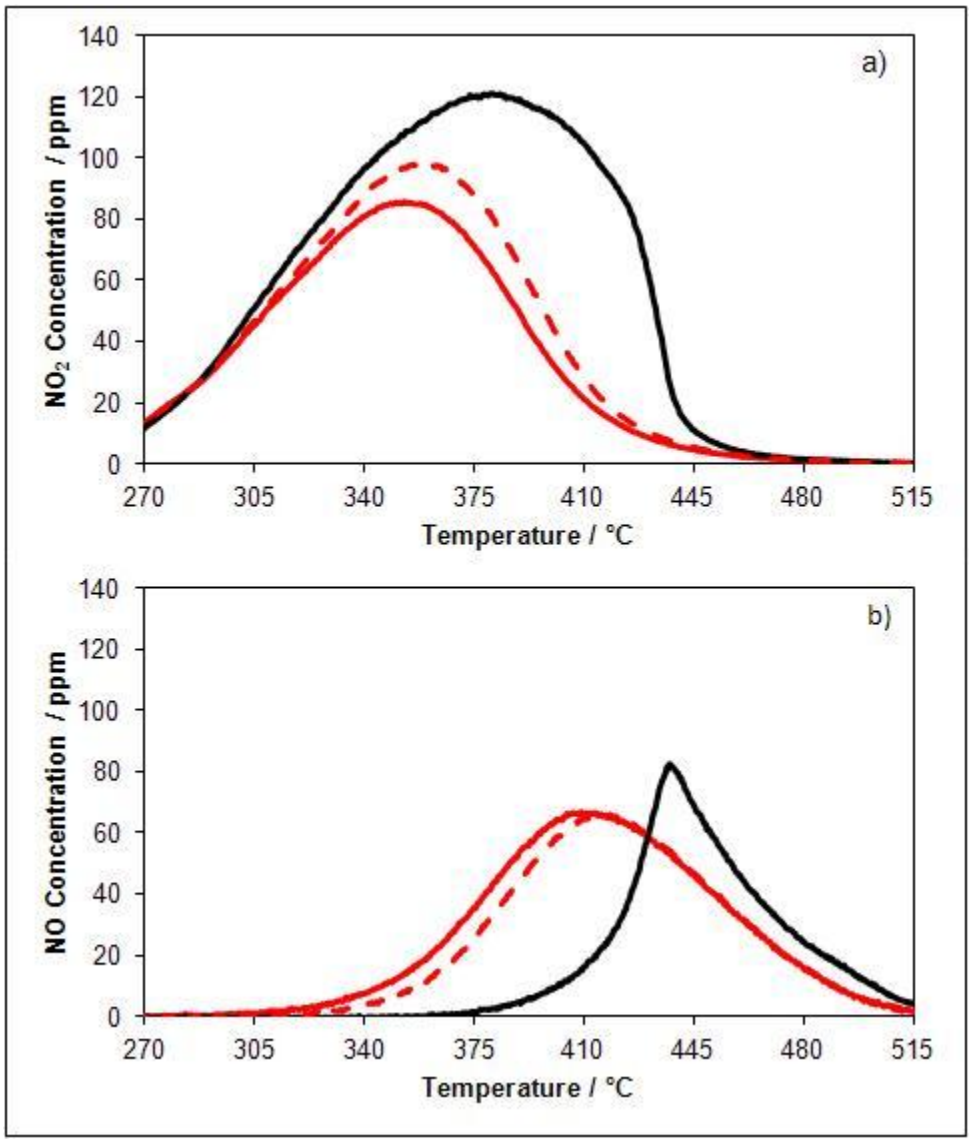

Figure 26: TPD of a) NO_2 and b) NO from 270 to 515℃ after flowing 1000 ppm NO_2, 6.5% O_2 and balance N_2 for 1.5 hours (solid black –), and after 6 pulses (dotted red: – –) and 15 pulses (solid red: –) of 20 ppm C_3H_6.

Based on Figure 26, less NO_2 and more NO were released during the TPD when the nitrates were exposed to C_3H_6. No N_2O was released during the TPD. However, peaks of N_2O, NO

and NO_2 were observed during each C_3H_6 pulse. A sample profile of the NO_x released during C_3H_6 pulsing is shown in Figure 27.

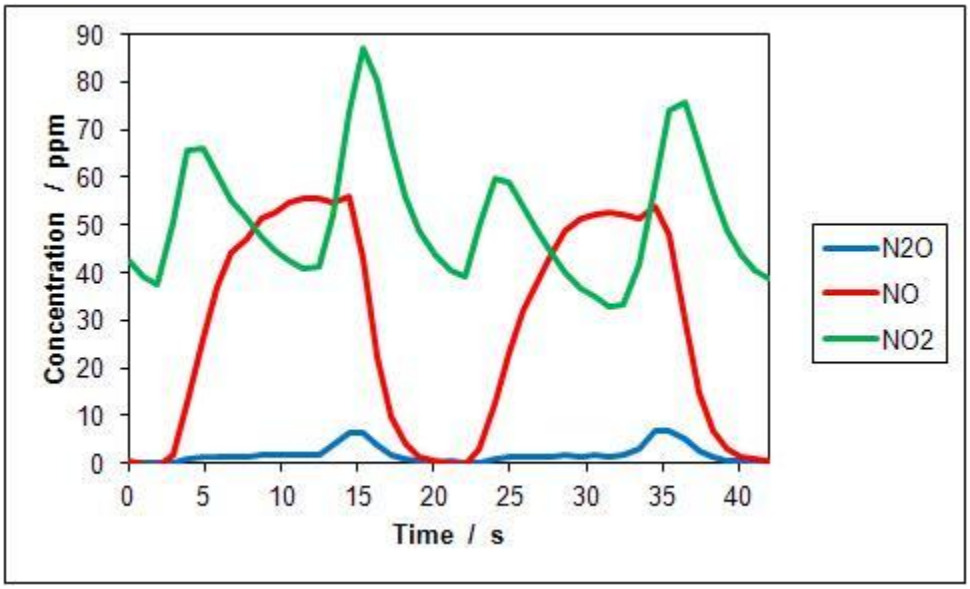

Figure 27: Sample profile of NO_x released during C_3H_6 pulsing.

The profiles of NO, NO_2 and N_2O in Figure 27 during C_3H_6 pulses indicate that C_3H_6 was reacting with the stored NO_x. N_2O is generally formed as a by-product when NO_x and HCs react over Pt/Al_2O_3 [80] and there is reported evidence suggesting that the N_2O production mechanism involves adsorbed NO species and surface HC species [23]. The integrated areas of the N_2O, NO and NO_2 released during each C_3H_6 pulse are displayed in Figure 28.

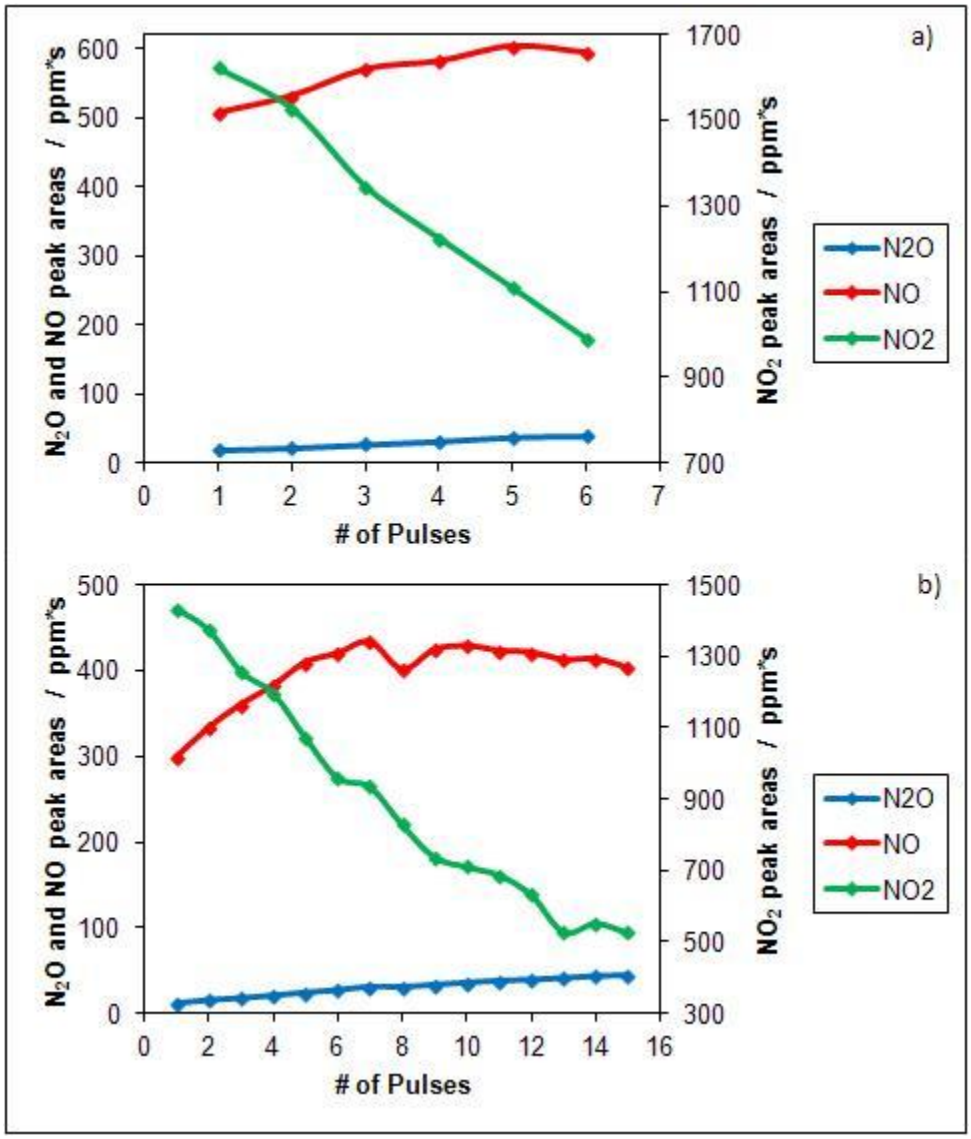

Figure 28: Amount of N_2O, NO and NO_2 released during each C_3H_6 pulse for a) 6 pulses and b) 15 pulses.

With an increasing number of C_3H_6 pulses, more NO_x was of course released. Of the total NO_x released, about 1.5% and 2.2% is formed as N_2O during C_3H_6 pulsing. The amount of N_2O and NO released increased while the amount of NO_2 released decreased with each C_3H_6 pulse. With an increasing C_3H_6 to NO_x ratio, more NO_2 can be reduced to NO, which

explains why the amount of NO released increased with each pulse, since with each pulse there is less surface NO_x species remaining. The amount of NO released with each pulse leveled off after around 7 pulses while N_2O continued to increase. This again is due to an increasing C_3H_6 to surface NO_x ratio. The ratios of the total amount of NO to NO_2 released were 0.43 and 0.45 for 6 and 15 pulses, respectively.

During the TPD, more NO and less NO_2 was released when the C_3H_6 pulsing step was performed beforehand, as shown in Figure 26. The degree of reduction depended on how much C_3H_6 was exposed to the surface NO_x. To quantify the degree of reduction, the integrated area of the NO and NO_2 peaks of the TPD are tabulated in Table V.

Table V: Total amount of NO, NO_2 and NO_x released during the TPDs.

TPD Type	NO (ppm*s)	NO_2 (ppm*s)	Total NO_x (ppm*s)
No Pulse	20273.93	76702.00	96975.93
6 Pulses	28484.88	52837.82	81322.70
15 pulses	31349.00	46731.12	78080.12

Around 79.1% of the released NO_x during the TPD without any exposure to C_3H_6 was released as NO_2 while 65.0% and 59.9% were released as NO_2 with 6 and 15 ten-second pulses of 20 ppm C_3H_6, respectively. Also, it is important to note that the total amounts of NO_x released were not the same in experiments with and without C_3H_6 pulses even though the same amount of NO_x should have been stored on the catalyst, which indicates that the

nitrates were reduced not just to nitrites, with NO_x release during TPD, but some were even further reduced to N_2 and N_2O.

A.3 Conclusions

DRIFTS experiments showed that nitrates get reduced to nitrites at lower temperatures and that Pt is required for this reaction to occur. TPD experiments validated that nitrates on the Pt/Al_2O_3 catalyst surface were reduced as more NO was released during the TPD than NO_2 when exposed to C_3H_6, and that some were even further reduced to N_2 as well.

Appendix B

Sample Calculations and Additional Data

B.1 Sample calculation for Pt dispersion (%)

- **Pt/SiO_2**

$$\text{Pt Dispersion (\%)}=\left(\frac{\frac{A_S}{N_S}-\frac{A_A}{N_A}}{\frac{A_S}{N_S}}\right)\cdot\left(\frac{V_{H_2}}{V_{STP}}\right)\cdot\left(\frac{\upsilon_{Pt:H_2}}{m_{cat}\cdot\omega_{Pt}}\right)\cdot M_{Pt}\cdot 100\%$$

Areas of the peaks of the pulses were calculated using OriginPro 7.0.

Pt Dispersion (%) =

$$\left(\frac{\frac{4.07711\times10^{-5}}{24}-\frac{3.1179\times10^{-6}}{2}}{\frac{4.07711\times10^{-5}}{24}}\right)\cdot\left(\frac{5\times10^{-6}\text{L}}{22.4\text{L/mol}}\right)\cdot\left(\frac{2}{0.045\text{ g Cat}\times 1\%\text{ Pt}}\right)\cdot 195.1\ \frac{\text{g}}{\text{mol}}\cdot 100\%$$

$$= \mathbf{1.6}\%$$

B.2 Additional Data – Reaction Kinetics

B.2.1 Pt/SiO_2

Table VI: Arrhenius plot data for C_3H_6 oxidation with O_2 by TPO over Pt/SiO_2.

Experiment 1		Repeat 1		Repeat 2		Repeat 3	
1/T (K^{-1})	**Ln X**	**1/T (K^{-1})**	**Ln X**	**1/T (K^{-1})**	**Ln X**	**1/T (K^{-1})**	**Ln X**
0.002748	2.04	0.002733	2.09	0.002726	1.97	0.002729	2.12
0.002745	2.08	0.002729	2.12	0.002709	2.33	0.002721	2.23
0.002733	2.23	0.002717	2.24	0.002703	2.33	0.002717	2.30
0.002729	2.30	0.002713	2.39	0.002698	2.47	0.002713	2.33
0.002725	2.41	0.002709	2.50	0.002694	2.49	0.002709	2.35
0.002718	2.52	0.002705	2.56	0.002689	2.59	0.002702	2.49
0.002715	2.43	0.002701	2.56	0.002684	2.64	0.002695	2.57
0.002711	2.57	0.002697	2.61	0.002679	2.75	0.002691	2.62
0.002708	2.56	0.002693	2.58			0.002688	2.67
0.002705	2.72	0.002689	2.66				
0.002700	2.73						

Table VII: Arrhenius plot data for C_3H_6 oxidation with O_2 by Step Ramp over Pt/SiO_2.

Experiment 1		Repeat 1	
1/T (K^{-1})	**Ln X**	**1/T (K^{-1})**	**Ln X**
0.002791	1.02	0.002792	0.82
0.002752	1.70	0.002753	1.54
0.002716	2.23	0.002716	2.18
0.002680	2.82	0.002679	2.75

Table VIII: Arrhenius plot data for C_3H_6 oxidation with NO_2 by TPO over Pt/SiO_2.

Experiment 1		Repeat 1		Repeat 2	
1/T (K^{-1})	Ln X	1/T (K^{-1})	Ln X	1/T (K^{-1})	Ln X
0.002563	2.06	0.002522	2.06	0.002501	2.03
0.002561	2.02	0.002518	2.08	0.002493	2.01
0.002557	2.04	0.002515	2.15	0.002489	2.02
0.002556	2.07	0.002512	2.02	0.002485	2.09
0.002553	2.05	0.002508	2.15	0.002481	2.13
0.002550	2.09	0.002500	2.27	0.002473	2.22
0.002548	2.19	0.002496	2.18	0.002462	2.37
0.002546	2.22	0.002492	2.25	0.002458	2.48
0.002543	2.27	0.002484	2.35	0.002455	2.49
0.002538	2.32	0.002481	2.40	0.002452	2.53
0.002535	2.32	0.002478	2.36	0.002449	2.53
0.002530	2.29	0.002474	2.48	0.002446	2.52
0.002528	2.33	0.002467	2.56	0.002440	2.53
0.002527	2.35	0.002464	2.58	0.002428	2.59
0.002525	2.39	0.002461	2.61	0.002425	2.67
0.002523	2.40	0.002457	2.56	0.002422	2.66
0.002520	2.49	0.002449	2.69	0.002418	2.74
0.002518	2.49				
0.002517	2.47				
0.002515	2.52				
0.002512	2.57				
0.002511	2.54				
0.002509	2.58				
0.002501	2.64				
0.002499	2.72				
0.002496	2.71				

Table IX: Arrhenius plot data for C_3H_6 oxidation with NO_2 by Step Ramp over Pt/SiO_2.

Experiment 1		Repeat 1	
1/T (K^{-1})	Ln X	1/T (K^{-1})	Ln X
0.002481	1.61	0.002391	2.14
0.002450	2.03	0.002363	2.42
0.002421	2.30	0.002336	2.68
0.002391	2.63	0.002308	2.89
0.002363	2.87		

B.2.2 Pt/Al_2O_3

Table X: Arrhenius plot data for C_3H_6 oxidation with O_2 by TPO over Pt/Al_2O_3.

Experiment 1		Repeat 1		Repeat 2		Repeat 3	
1/T (K^{-1})	Ln X	1/T (K^{-1})	Ln X	1/T (K^{-1})	Ln X	1/T (K^{-1})	Ln X
0.002745	2.17	0.002743	2.01	0.002740	2.05	0.002755	2.04
0.002744	2.18	0.002739	2.08	0.002736	2.22	0.002748	2.06
0.002741	2.21	0.002733	2.21	0.002727	2.29	0.002745	2.12
0.002730	2.35	0.002729	2.24	0.002718	2.43	0.002738	2.28
0.002726	2.39	0.002726	2.37	0.002714	2.47	0.002734	2.43
0.002725	2.42	0.002722	2.52	0.002707	2.60	0.002730	2.41
0.002723	2.46	0.002719	2.54	0.002703	2.70	0.002727	2.47
0.002721	2.51	0.002715	2.49			0.002723	2.61
0.002719	2.54	0.002713	2.54			0.002719	2.56
0.002717	2.55	0.002709	2.68			0.002715	2.64
0.002716	2.59	0.002706	2.68			0.002712	2.67
0.002713	2.65						
0.002711	2.67						
0.002709	2.70						

Table XI: Arrhenius plot data for C_3H_6 oxidation with O_2 by Step Ramp over Pt/Al_2O_3.

Experiment 1		Repeat 1		Repeat 2	
1/T (K^{-1})	Ln X	1/T (K^{-1})	Ln X	1/T (K^{-1})	Ln X
0.002791	0.66	0.002769	1.29	0.002792	1.35
0.002754	1.53	0.002754	1.63	0.002769	1.60
0.002715	2.17	0.002738	1.90	0.002754	1.87
0.002680	2.89	0.002716	2.26	0.002739	2.14
		0.002695	2.60	0.002716	2.41

Table XII: Arrhenius plot data for C_3H_6 oxidation with NO_2 by TPO over Pt/Al_2O_3.

Experiment 1		Repeat 1		Repeat 2		Repeat 3	
1/T (K^{-1})	Ln X	1/T (K^{-1})	Ln X	1/T (K^{-1})	Ln X	1/T (K^{-1})	Ln X
0.002619	2.05	0.002606	2.09	0.002614	2.02	0.002625	2.01
0.002615	2.06	0.002602	2.15	0.002612	2.11	0.002620	2.05
0.002611	2.17	0.002599	2.10	0.002611	2.08	0.002619	2.00
0.002607	2.17	0.002595	2.16	0.002607	2.18	0.002615	2.06
0.002604	2.15	0.002588	2.33	0.002603	2.17	0.002611	2.20
0.002600	2.32	0.002580	2.46	0.002599	2.31	0.002610	2.17
0.002597	2.34	0.002576	2.53	0.002597	2.39	0.002608	2.20
0.002593	2.45	0.002572	2.57	0.002595	2.34	0.002606	2.25
0.002589	2.53	0.002568	2.53	0.002593	2.30	0.002598	2.31
0.002585	2.46	0.002564	2.58	0.002590	2.39	0.002596	2.28
0.002582	2.65	0.002560	2.75	0.002587	2.50	0.002593	2.39
0.002578	2.69	0.002556	2.74	0.002586	2.47	0.002590	2.35
0.002574	2.68			0.002584	2.50	0.002589	2.36
0.002570	2.74			0.002576	2.65	0.002587	2.45
				0.002574	2.62	0.002582	2.58
				0.002572	2.71	0.002580	2.58
				0.002570	2.77	0.002578	2.62
				0.002569	2.74	0.002574	2.67

Table XIII: Arrhenius plot data for C_3H_6 oxidation with NO_2 by Step Ramp over Pt/Al_2O_3.

Experiment 1		Repeat 1		Repeat 2	
1/T (K^{-1})	Ln X	1/T (K^{-1})	Ln X	1/T (K^{-1})	Ln X
0.002576	1.54	0.002645	1.40	0.002609	1.40
0.002544	2.11	0.002610	1.87	0.002577	1.77
0.002511	2.63	0.002576	2.26	0.002556	2.04
0.002481	3.00	0.002545	2.64	0.002544	2.20
				0.002524	2.43

Table XIV: Arrhenius plot data for C_3H_6 oxidation with O_2 and Nitrates by TPO over Pt/Al_2O_3.

Experiment 1		Repeat 1		Repeat 2		Repeat 3	
1/T (K^{-1})	Ln X	1/T (K^{-1})	Ln X	1/T (K^{-1})	Ln X	1/T (K^{-1})	Ln X
0.002860	2.07	0.002857	2.11	0.002850	2.20	0.002859	2.04
0.002856	2.09	0.002856	2.11	0.002849	2.20	0.002857	2.08
0.002854	2.11	0.002854	2.17	0.002847	2.24	0.002857	2.09
0.002853	2.19	0.002851	2.15	0.002842	2.33	0.002856	2.07
0.002852	2.20	0.002847	2.25	0.002842	2.34	0.002856	2.07
0.002850	2.21	0.002846	2.25	0.002841	2.34	0.002855	2.09
0.002848	2.18	0.002843	2.33	0.002839	2.35	0.002855	2.08
0.002848	2.20	0.002841	2.31	0.002839	2.35	0.002851	2.12
0.002847	2.19	0.002839	2.39	0.002838	2.37	0.002850	2.15
0.002847	2.26	0.002837	2.31	0.002835	2.39	0.002850	2.19
0.002846	2.26	0.002835	2.33	0.002834	2.43	0.002849	2.18
0.002845	2.20	0.002833	2.39	0.002833	2.47	0.002848	2.16
0.002844	2.28	0.002829	2.42	0.002832	2.46	0.002847	2.21
0.002843	2.29	0.002828	2.49	0.002830	2.50	0.002846	2.19
0.002843	2.27	0.002821	2.52	0.002827	2.53	0.002846	2.17
0.002842	2.27	0.002819	2.56	0.002826	2.52	0.002844	2.21
0.002841	2.29	0.002817	2.64	0.002825	2.52	0.002843	2.21
0.002841	2.34	0.002816	2.64	0.002824	2.53	0.002842	2.25
0.002840	2.36	0.002815	2.61	0.002822	2.56	0.002839	2.28
0.002839	2.35	0.002811	2.67	0.002820	2.56	0.002836	2.33
0.002839	2.37	0.002810	2.71	0.002819	2.61	0.002836	2.33
0.002838	2.37			0.002818	2.61	0.002833	2.36
0.002837	2.36			0.002817	2.64	0.002833	2.35
0.002837	2.37			0.002816	2.64	0.002831	2.33
0.002836	2.34			0.002814	2.64	0.002829	2.35
0.002834	2.38			0.002812	2.72	0.002827	2.43
0.002833	2.41					0.002827	2.40
0.002833	2.39					0.002824	2.48
0.002831	2.42					0.002823	2.45
0.002830	2.47					0.002822	2.47
0.002830	2.42					0.002820	2.47
0.002829	2.43					0.002819	2.51
0.002828	2.49					0.002819	2.50
0.002828	2.43					0.002816	2.58
0.002827	2.50					0.002815	2.58
0.002826	2.53					0.002814	2.56
0.002826	2.51					0.002813	2.57
0.002825	2.48					0.002811	2.60
0.002824	2.53					0.002811	2.60
0.002823	2.55					0.002810	2.60
0.002823	2.54					0.002808	2.67
0.002822	2.55					0.002807	2.63
0.002821	2.57					0.002806	2.65
0.002821	2.58					0.002806	2.66
0.002820	2.60					0.002803	2.69
0.002819	2.57					0.002803	2.69
0.002817	2.63					0.002802	2.70
0.002815	2.63					0.002801	2.72
0.002815	2.63						
0.002814	2.65						
0.002814	2.68						
0.002813	2.70						
0.002811	2.68						
0.002809	2.70						
0.002808	2.69						
0.002807	2.70						
0.002806	2.71						
0.002806	2.74						
0.002805	2.76						
0.002803	2.77						

B.3 Sample Calculations – Activation Energy, Errors and t-test

B.3.1 Activation Energy and Error Calculations

Using the data set of C_3H_6 oxidation with O_2 by TPO over Pt/SiO_2 in Table VI, sample calculations of activation energy and the error of the slope are shown.

The linear set of data can be fitted with the following equation: $LnX = A_0 + A_1 \cdot 1/T$

A model with 2 parameters (p): slope and intercept; A_1 and A_0, respectively.

And from the Arrhenius equation, the slope represents – E/R.

The repeated experiment data is combined into one data set as they are the same experiment done independently. This way the error can be just calculated from the error of the slope.

In matrix form the 1/T and lnX data set transforms to the following:

1/T	Ln X
0.002729	2.115484
0.002721	2.229184
0.002717	2.295103
0.002713	2.329219
0.002709	2.34557
0.002702	2.486772
0.002695	2.56912
0.002691	2.62341
0.002688	2.666611
0.002733	2.089547
0.002729	2.12122
0.002717	2.243153
0.002713	2.391564
0.002709	2.502966
0.002705	2.562207
0.002701	2.564913
0.002697	2.609194
0.002693	2.581541
0.002689	2.655565

$$[X] = \begin{bmatrix} 1 & 0.002729 \\ 1 & 0.002721 \\ 1 & 0.002717 \\ 1 & 0.002713 \\ 1 & 0.002709 \\ 1 & 0.002702 \\ 1 & 0.002695 \\ 1 & 0.002691 \\ 1 & 0.002688 \\ 1 & 0.002733 \\ 1 & 0.002729 \\ 1 & 0.002717 \\ 1 & 0.002713 \\ 1 & 0.002709 \\ 1 & 0.002705 \\ 1 & 0.002701 \\ 1 & 0.002697 \\ 1 & 0.002693 \\ 1 & 0.002689 \end{bmatrix} \qquad [Y] = \begin{bmatrix} 2.115484 \\ 2.229184 \\ 2.295103 \\ 2.329219 \\ 2.34557 \\ 2.486772 \\ 2.56912 \\ 2.62341 \\ 2.666611 \\ 2.089547 \\ 2.12122 \\ 2.243153 \\ 2.391564 \\ 2.502966 \\ 2.562207 \\ 2.564913 \\ 2.609194 \\ 2.581541 \\ 2.655565 \end{bmatrix}$$

n = 19, p = 2

General Linear Regression formulas are shown below:

Parameter matrix: $[A] = (X'X)^{-1} (X'Y)$ outputs A_0 and A_1

Sum of squares error: $SSE = Y'Y - A'(X'Y)$

Sum of squares regression: $SSR = A'(X'Y) - nYavg^2$

Sum of squares Total: $SST = Y'Y - nYavg^2$

Sample Variance: $s^2 = SSE / (n - p)$

$R^2 = SSR / SST$

Confidence interval (CI): $A_i \pm t_{\alpha/2,\, n\text{-}p} \cdot \sqrt{s^2 (X'X)^{-1}_{i+1,i+1}}$

$$[X'X] = \begin{bmatrix} 19 & 0.051450444 \\ 0.05145 & 1.39327 \times 10^{-4} \end{bmatrix} \qquad [X'X]^{-1} = \begin{bmatrix} 2074.971 & -766241 \\ -766241 & 282963221 \end{bmatrix}$$

$[X'Y] = \begin{bmatrix} 45.98234 \\ 0.124469 \end{bmatrix}; [A] = \begin{bmatrix} 39.08288 \\ -13539.1 \end{bmatrix}; [Y'Y] = [111.9664]\ ;\ A'[X'Y] =$

$[111.9308]\ ; Y_{avg} = 2.420123$

A_1 = **-13539.1** is the slope

Therefore $\mathbf{E} = -13539.1\ \text{K} \cdot 8.314 \frac{\text{J}}{\text{mol K}} \Big/ 1000 \frac{\text{J}}{\text{kJ}} = \mathbf{112.564} \frac{\mathbf{kJ}}{\mathbf{mol}}$

$SSE = 111.9664 - 111.9308 = 0.035636$

$SSR = 111.9308 - 19(2.420123)^2 = 0.647812$

$SST = 0.035636 + 0.647812 = 0.683447934$

$R^2 = \frac{SSR}{SST} = \frac{0.647812}{0.683447934} = \mathbf{0.947859}$

$s^2 = \frac{SSE}{n-p} = \frac{0.035636}{19-2} = 0.002096$

$[X'X]_{22}^{-1} = 282963221$

Confidence interval: $A_i \pm t_{\frac{\alpha}{2},n-p} \cdot \sqrt{s^2 (X'X)_{i+1,i+1}^{-1}}$

At 95% Confidence level ($\alpha = 0.05$):

$t_{\frac{\alpha}{2},n-p} = t_{0.025,19-2} = 2.458051$

$A_1 \pm 2.458051 \cdot \sqrt{(0.002096)(282963221)} = -13539.1 \pm 1893.103$

Therefore, E = 112.564 ± 15.73926 kJ/mol

Same method of calculation is used for the rest of the experiments and they are listed in Table XV.

Table XV: Activation energies of each experiment/oxidation reactions and all the intermediate calculation values.

Experiment Type / Catalyst	n	s^2	$(X'X)^{-1}_{2,2}$	$t_{\frac{\alpha}{2},n-p}$	A_1	R^2	CI	E
$C_3H_6 + O_2$ TPO Pt/SiO_2	19	0.00210	2.83E+08	2.46	-13539.1	0.9479	1893.1	112.56 ± 15.74
$C_3H_6 + O_2$ TPO Pt/Al_2O_3	22	0.00275	2.60E+08	2.42	-17310.9	0.9545	2048.8	143.92 ± 17.03
$C_3H_6 + O_2$ Step Ramp Pt/SiO_2	8	0.00572	7.19E+07	2.97	-16577.6	0.9911	1904.4	137.83 ± 15.83
$C_3H_6 + O_2$ Step Ramp Pt/Al_2O_3	14	0.00561	7.14E+07	2.56	-15782.3	0.9811	1620.3	131.21 ± 13.47
$C_3H_6 + NO_2$ TPO Pt/SiO_2	60	0.00231	1.16E+07	2.30	-9972.5	0.9853	376.8	82.91 ± 3.13
$C_3H_6 + NO_2$ TPO Pt/Al_2O_3	50	0.00240	8.44E+07	2.31	-14444.1	0.9555	1040.6	120.09 ± 8.65
$C_3H_6 + NO_2$ Step Ramp Pt/SiO_2	9	0.00195	4.21E+08	2.84	-10303.7	0.9946	813.9	85.67 ± 6.77
$C_3H_6 + NO_2$ Step Ramp Pt/Al_2O_3	13	0.00639	4.25E+07	2.59	-13336.9	0.9835	1351.5	110.88 ± 11.24
$C_3H_6 + O_2$ + Nitrates TPO	155	0.00449	2.67E+07	2.26	-12046.2	0.9765	784.5	100.15 ± 6.52

The activation energies of individual repeated experiments were also calculated and averaged and the variances between the repeated experiments were calculated with the following equation.

$$s^2 = \left(\frac{1}{n-1}\right) \cdot \left\{ \sum_{k=1}^{n} E_i^2 - n\left(\sum_{k=1}^{n} E_i\right)^2 \right\}$$

Sample calculations using Pt/SiO_2 $C_3H_6 + O_2$ Step Ramp:

n = 2

$E_{average}$ = 132.99 + 142.45 / 2 = 137.72 kJ/mol

$$s^2 = \left(\frac{1}{2-1}\right) \cdot \left\{ \sum_{k=1}^{n} (17686.14 + 20292.75) - 2\left(\sum_{k=1}^{n} 132.99 + 142.45 \right)^2 \right\}$$

$$E_{average} = \mathbf{137.72}$$

$$s^2 = \mathbf{44.78}$$

Same method of calculation is used for the rest of the experiments and they are listed in Table XVI.

Table XVI: Average activation energies and variances between experiment repeats.

Experiment Type / Catalyst	Expt #	E	s^2	Eavg
$C_3H_6 + O_2$ TPO Pt/SiO_2	Expt 1	119.94	91.20	119.69
	Repeat 1	114.36		
	Repeat 2	133.01		
	Repeat 3	111.47		
$C_3H_6 + O_2$ TPO Pt/Al_2O_3	Expt 1	123.51	160.20	135.67
	Repeat 1	153.34		
	Repeat 2	131.29		
	Repeat 3	134.53		
$C_3H_6 + O_2$ Step Ramp Pt/SiO_2	Expt 1	132.99	44.78	137.72
	Repeat 1	142.45		
$C_3H_6 + O_2$ Step Ramp Pt/Al_2O_3	Expt 1	164.28	550.81	142.28
	Repeat 1	145.00		
	Repeat 2	117.58		
$C_3H_6 + NO_2$ TPO Pt/SiO_2	Expt 1	87.82	47.46	79.96
	Repeat 1	74.99		
	Repeat 2	77.06		
$C_3H_6 + NO_2$ TPO Pt/Al_2O_3	Expt 1	127.4	96.11	119.91
	Repeat 1	113.94		
	Repeat 2	129.03		
	Repeat 3	109.26		
$C_3H_6 + NO_2$ Step Ramp Pt/SiO_2	Expt 1	88.52	76.25	82.34
	Repeat 1	76.17		
$C_3H_6 + NO_2$ Step Ramp Pt/Al_2O_3	Expt 1	127.82	217.16	110.80
	Repeat 1	102.36		
	Repeat 2	102.23		
$C_3H_6 + O_2$ + Nitrates TPO Pt/Al_2O_3	Expt 1	104.43	16.77	101.63
	Repeat 1	95.97		
	Repeat 2	104.84		
	Repeat 3	101.27		

B.3.2 t-test calculations

To compare the activation energies calculated for C_3H_6 oxidation with different oxidants and between TPO and step ramp method, t-test at 95% confidence level was used.

A sample calculation is shown for O_2 vs NO_2 on Pt/SiO_2.

$C_3H_6 + O_2$ Step Ramp Pt/SiO_2	Expt 1	132.99
	Repeat 1	142.45
$C_3H_6 + NO_2$ Step Ramp Pt/SiO_2	Expt 1	88.52
	Repeat 1	76.17

$$s^2 = \left(\frac{1}{n-1}\right) \cdot \left\{\sum_{k=1}^{n} E_i^2 - n\left(\sum_{k=1}^{n} E_i\right)^2\right\}$$

$$s_{O_2}^2 = \left(\frac{1}{2-1}\right) \cdot \left\{(132.99^2 + 142.45^2) - 2\left(\frac{132.99 + 142.45}{2}\right)^2\right\} = 44.78$$

$$s_{NO_2}^2 = \left(\frac{1}{2-1}\right) \cdot \left\{(88.52^2 + 76.17^2) - 2\left(\frac{88.52 + 76.17}{2}\right)^2\right\} = 76.25$$

H_0: $E_{O_2} - E_{NO_2} = 0$

H_1: $E_{O_2} - E_{NO_2} \neq 0$

$$s_{pooled}^2 = \frac{(2-1) \cdot 44.78 + (2-1) \cdot 76.25}{2 + 2 - 2} = 60.51$$

$$T_{obs} = \frac{E_{O_2} - E_{NO_2} - 0}{\sqrt{s_{pooled}^2 \cdot \left(\frac{1}{n_1} + \frac{1}{n_2}\right)}} = \frac{137.72 - 82.34 - 0}{\sqrt{60.51 \cdot \left(\frac{1}{2} + \frac{1}{2}\right)}} = 7.119$$

$$t_{critical} = t_{\frac{0.05}{2},4+3-2} = 6.205347$$

$$t_{critical} < T_{obs}$$

Therefore, it can be said with 95% confidence that the activation energies calculated between O_2 and NO_2 are significantly different for the experiment done on Pt/SiO_2.

Same calculation method was used to determine whether the calculated activation energies are different between oxidants, supports, and methods (TPO vs Step Ramp). When T_{obs} is less than $t_{critical}$, then there is a significant difference between the two being compared.

Permission

SPRINGER LICENSE
TERMS AND CONDITIONS

Aug 23, 2012

This is a License Agreement between Hyunsuk Oh ("You") and Springer ("Springer") provided by Copyright Clearance Center ("CCC"). The license consists of your order details, the terms and conditions provided by Springer, and the payment terms and conditions.

License Number	2974970557335
License date	Aug 23, 2012
Licensed content publisher	Springer
Licensed content publication	Catalysis Letters
Licensed content title	NO Oxidation Inhibition by Hydrocarbons over a Diesel Oxidation Catalyst: Reaction Between Surface Nitrates and Hydrocarbons
Licensed content author	Harry Oh
Licensed content date	Jan 1, 2011
Volume number	141
Issue number	12
Type of Use	Thesis/Dissertation
Portion	Full text
Number of copies	1
Author of this Springer article	Yes and you are the sole author of the new work
Order reference number	
Title of your thesis / dissertation	C3H6/NOx Interactions Over a Diesel Oxidation Catalyst: Hydrocarbon Oxidation Reaction Pathways

Expected completion date	Oct 2012
Estimated size(pages)	100
Total	0.00 CAD